Munc13-4 interacts with syntaxin 7 and regulates late endosomal maturation, endosomal signaling, and TLR9-initiated cellular responses

Jing He[a], Jennifer L. Johnson[a], Jlenia Monfregola[a], Mahalakshmi Ramadass[a], Kersi Pestonjamasp[b], Gennaro Napolitano[a], Jinzhong Zhang[a], and Sergio D. Catz[a]

[a]Department of Molecular and Experimental Medicine, Scripps Research Institute, La Jolla, CA 92037; [b]Cancer Center Microscopy Shared Resource, University of California, San Diego, La Jolla, CA 92093

ABSTRACT **The molecular mechanisms that regulate late endosomal maturation and function are not completely elucidated, and direct evidence of a calcium sensor is lacking. Here we identify a novel mechanism of late endosomal maturation that involves a new molecular interaction between the tethering factor Munc13-4, syntaxin 7, and VAMP8. Munc13-4 binding to syntaxin 7 was significantly increased by calcium. Colocalization of Munc13-4 and syntaxin 7 at late endosomes was demonstrated by high-resolution and live-cell microscopy. Munc13-4–deficient cells show increased numbers of significantly enlarged late endosomes, a phenotype that was mimicked by the fusion inhibitor chloroquine in wild-type cells and rescued by expression of Munc13-4 but not by a syntaxin 7–binding–deficient mutant. Late endosomes from Munc13-4-KO neutrophils show decreased degradative capacity. Munc13-4–knockout neutrophils show impaired endosomal-initiated, TLR9-dependent signaling and deficient TLR9-specific CD11b up-regulation. Thus we present a novel mechanism of late endosomal maturation and propose that Munc13-4 regulates the late endocytic machinery and late endosomal–associated innate immune cellular functions.**

Monitoring Editor
Thomas F. J. Martin
University of Wisconsin

Received: May 18, 2015
Revised: Oct 16, 2015
Accepted: Dec 8, 2015

INTRODUCTION

Late endosomes (LEs) are intracellular organelles of the endocytic pathway that have multiple important roles in the regulation of cellular homeostasis and specialized cellular functions (Luzio *et al.*, 2010; Huotari and Helenius, 2011). LEs control cellular processes as diverse as signaling, protein degradative pathways, receptor maturation, phagosomal maturation, and autophagy. In addition, many pathogens use the endocytic pathway and in particular late endosomes to avert host defense mechanisms. Thus LEs regulate important processes of the innate immune response (Gruenberg and van der Goot, 2006).

Late endosomes are dynamic organelles, in terms of both subcellular distribution and movement, and are heterogeneous in composition according to their maturation state (Gruenberg and Stenmark, 2004; Huotari and Helenius, 2011). Thus they are formed from early endosomes as large vesicles and undergo a process of maturation that involves a small Rab GTPase conversion (from RAB5 to RAB7; Rink *et al.*, 2005), as well as other molecular and structural changes, including the formation of intraluminal vesicles induced by lysobisphosphatidic acid (Matsuo *et al.*, 2004), lipidic modifications, acquisition of lysosomal-associated membrane proteins (LAMPs), and phosphatidylinositol phosphate conversion (phosphatidylinositol 3-phosphate to phosphatidylinositol 3,5-bisphosphate switch; Huotari and Helenius, 2011).

A central process in LE function is represented by the fusion of this organelle with lysosomes (Luzio *et al.*, 2010), a mechanism necessary for endocytic substrate processing and macromolecule degradation. The now-accepted mechanism consists of the fusion of LEs with lysosomes either by "kiss-and-run" or partial fusion, leading to the delivery of lysosomal content into LEs (Luzio *et al.*, 2007). In addition, LEs undergo homotypic fusion events that help reshape

This article was published online ahead of print in MBoC in Press (http://www.molbiolcell.org/cgi/doi/10.1091/mbc.E15-05-0283) December 17, 2015.

J.H., J.L.J., and J.M. performed experiments, analyzed data, and contributed ideas and comments; M.R. performed experiments and contributed ideas and comments; K.J. performed experiments; G.N. and J.Z. contributed ideas and comments; S.D.C. designed and performed experiments, analyzed data, and wrote the manuscript with input from J.H. and J.L.J.

Address correspondence to: Sergio D. Catz (scatz@scripps.edu).

Abbreviations used: CoIP, coimmunoprecipitation; CQ, chloroquine; FITC, fluorescein isothiocyanate; ILV, intraluminal vesicles; LAMP, lysosomal-associated membrane proteins; LEs, late endosomes; LRO, lysosome-related organelle; MPO, myeloperoxidase; MVB, multivesicular bodies; RPE, retinal pigment epithelial; SNAREs, soluble *N*-ethylmaleimide–sensitive factor attachment protein receptors; STORM, stochastic optical reconstruction microscopy; STX, syntaxin; TIRF, total internal reflection fluorescence; VAMPs, vesicle-associated membrane proteins; Vti1b, vesicle transport through interaction with t-SNAREs; WT, wild type.

the morphology of these organelles (Luzio *et al.*, 2010). Both heterotypic lysosome-late endosome fusion and homotypic fusion of late endosomes are maturation processes tightly regulated by soluble *N*-ethylmaleimide sensitive factor attachment protein receptors (SNAREs; Pryor *et al.*, 2004) and other accessory proteins, including the small GTPase RAB7 and the mammalian homotypic fusion and vacuole protein sorting (HOPS) complex (Kim *et al.*, 2001).

Syntaxin 7 is a Q-SNARE that participates in the formation of the assembled "*trans*"-SNARE complex during both homotypic and heterotypic fusion (Pryor *et al.*, 2004). The R-SNAREs vesicle-associated membrane proteins 7 and 8 (VAMP7 and VAMP8) are able to form *trans*-SNARE complexes with syntaxin 7 and regulate LE fusion (Mullock *et al.*, 2000; Pryor *et al.*, 2004). The Qb-SNARE Vti1b is also known to participate in this process (Antonin *et al.*, 2000). In addition to SNARE assembly, fusion of late endosomes with lysosomes requires calcium release from the lumen of these organelles (Pryor *et al.*, 2000), and, similar to yeast homotypic vacuole fusion (Peters and Mayer, 1998), it requires the regulatory molecule calmodulin (Pryor *et al.*, 2000). The molecular mechanisms regulating calcium-dependent LE maturation are not fully understood, however, and the participation of additional regulatory factors in this process is plausible.

Munc13-4 is a tethering, docking, and fusion regulator known to participate in the secretory pathway of several cellular systems (Feldmann *et al.*, 2003; Brzezinska *et al.*, 2008; Johnson *et al.*, 2010; Elstak *et al.*, 2011). It is highly expressed in hematopoietic cells and also in lungs, kidneys, and other organs with secretory functions (Koch *et al.*, 2000). Although originally described as an effector of the small GTPase Rab27a for the regulation of lysosome-related organelle (LRO) exocytosis (Shirakawa *et al.*, 2004), Munc13-4 also regulates Rab27a-independent mechanisms (Menager *et al.*, 2007; Johnson *et al.*, 2010; Monfregola *et al.*, 2012). Munc13-4 is well characterized as a modulator of the exocytosis of lysosome-related organelles in hematopoietic cells, including cytotoxic T lymphocytes, NK cells, neutrophils, basophils, and platelets (Feldmann *et al.*, 2003; Goishi *et al.*, 2004; Shirakawa *et al.*, 2004; Neeft *et al.*, 2005; Pivot-Pajot *et al.*, 2008; Johnson *et al.*, 2010). Munc13-4 contains two Munc-homology domains and two C2 domains (Koch *et al.*, 2000). The Munc13-4 C2 domains specifically interact with calcium and regulate exocytosis in a calcium- and SNARE-dependent manner (Boswell *et al.*, 2012). In addition, Munc13-4 is able to bind to phospholipids through its C2 domains (Pivot-Pajot *et al.*, 2008).

Neutrophils are central regulators of the innate immune response and control and eradicate infections by combating bacteria and fungi (Segal, 2005). Most neutrophil functions are regulated by their multiple intracellular storage organelles, including the azurophilic granule, a lysosome-related organelle (Borregaard *et al.*, 1993). On fusion of these organelles with the plasma membrane or with phagosomes, LROs deliver their cargo content, including the oxidative enzyme myeloperoxidase (MPO; Klebanoff, 2005) and the degradative enzyme cathepsin G, thus contributing to the killing of microorganisms either extracellularly or in the phagolysosome (Lee *et al.*, 2003). Few studies, however, have focused on the presence of LEs in neutrophils, and the formation and function of LEs in neutrophils remains unclear. Using gold-conjugated bovine serum albumin (BSA) and human neutrophils, Berger *et al.* (1994) demonstrated the presence of LEs/multivesicular bodies (MVBs) in these cells, which was further manifested upon activation of the endocytic pathway with the bacteria-derived peptide fMLP. Later Cieutat *et al.* (1998) also described MVBs and multilaminar compartments and suggested that they function as LEs, organelles that are different from the LROs in neutrophils. Both works characterized LAMP1 (and LAMP2) as specific LE markers in neutrophils, whereas LAMP3 (CD63) is a well-established azurophilic granule marker (Kuijpers *et al.*, 1991). Our research showing that Munc13-4–deficient cells are characterized by impaired LE–phagosomal fusion suggested that Munc13-4 function is not limited to the exocytic pathway and highlighted a possible role for Munc13-4 in LE function (Monfregola *et al.*, 2012).

In this work, we show that Munc13-4 is a syntaxin 7 binding protein and an important regulator of LE maturation. In addition, we show that Munc13-4 regulates endosome-initiated, TLR9-dependent signaling and TLR9-specific cellular functions in neutrophils. Thus Munc13-4 is a central regulator of the late endocytic machinery and its associated innate immune cellular functions.

RESULTS

Munc13-4 regulates late endosomal maturation

We showed that, in addition to exocytic defects, cells lacking Munc13-4 are characterized by impaired delivery of late endosomal proteins to the phagosome in neutrophils (Monfregola *et al.*, 2012). However, a possible function of Munc13-4 in late endosome regulation has not been previously investigated. Here we sought to address whether Munc13-4 is important for late endosome maturation. Because the detection and study of LEs in neutrophils has been elusive likely due to the effect of chemical fixatives on the size, shape, and structural conservation of LEs and intraluminal vesicles (Murk *et al.*, 2003), we studied LE maturation and dynamics in live cells. Because neutrophils are nondividing cells with a short half-life, we transfected neutrophils by nucleofection (Johnson *et al.*, 2012) and analyzed the spatiotemporal distribution of the LE marker enhanced green fluorescent protein (EGFP)–LAMP1 by pseudo–total internal reflection fluorescence microscopy (pTIRFM; Mudrakola *et al.*, 2009). In Figure 1A and Supplemental Movie S1, we show that LAMP1 is distributed at the limiting membrane of large vesicles that resemble late endosomes. In addition, we detected LAMP1 at puncta, reflecting its distribution at smaller compartments (Figure 1A and Supplemental Movie S1) that in electron microscopy studies correspond to electron-dense structures resembling conventional lysosomes (shown later). Quantitative analysis established that most transfected cells (83% of wild-type neutrophils and 97% of Munc13-4–deficient neutrophils) contain at least three LAMP1-positive large vesicles decorated with LAMP1 at the limiting membrane, giving the vesicles a hollow appearance. Similar distribution of LAMP1 was observed in retinal pigment epithelial (RPE) cells when transfected using lipids and analyzed 48 h after transfection (Figure 1B and Supplemental Movie S2), indicating that the distribution of LAMP1 at the limiting membrane of large late endosomes is independent of cell type, transfection method, and time of analysis after transfection. Electron microscopy studies demonstrate that LAMP1 is distributed at multilaminar vesicles and multivesicular bodies (Figure 1C), structures that were previously suggested to function as late endosomes in neutrophils (Cieutat *et al.*, 1998). In fact, Berger *et al.* (1994) demonstrated that MVBs at early stages of endocytosis lack LAMP1 but acquire LAMP1 at later stages, consistent with the idea that LAMP1-positive, large MVBs correspond to late but not early endosomes in neutrophils. In agreement with previous studies (Cieutat *et al.*, 1998), LAMP1 was not detected at secretory granules or lysosome-related organelles in neutrophils by immuno–electron microscopy (Figure 1C and Supplemental Figure S1). Instead, in addition to their distribution at LEs, we observed LAMP1-positive staining at relatively electron-dense small organelles in mouse neutrophils that resemble conventional lysosomes (Figure 1C) and most likely correspond to the punctate LAMP1 staining observed in

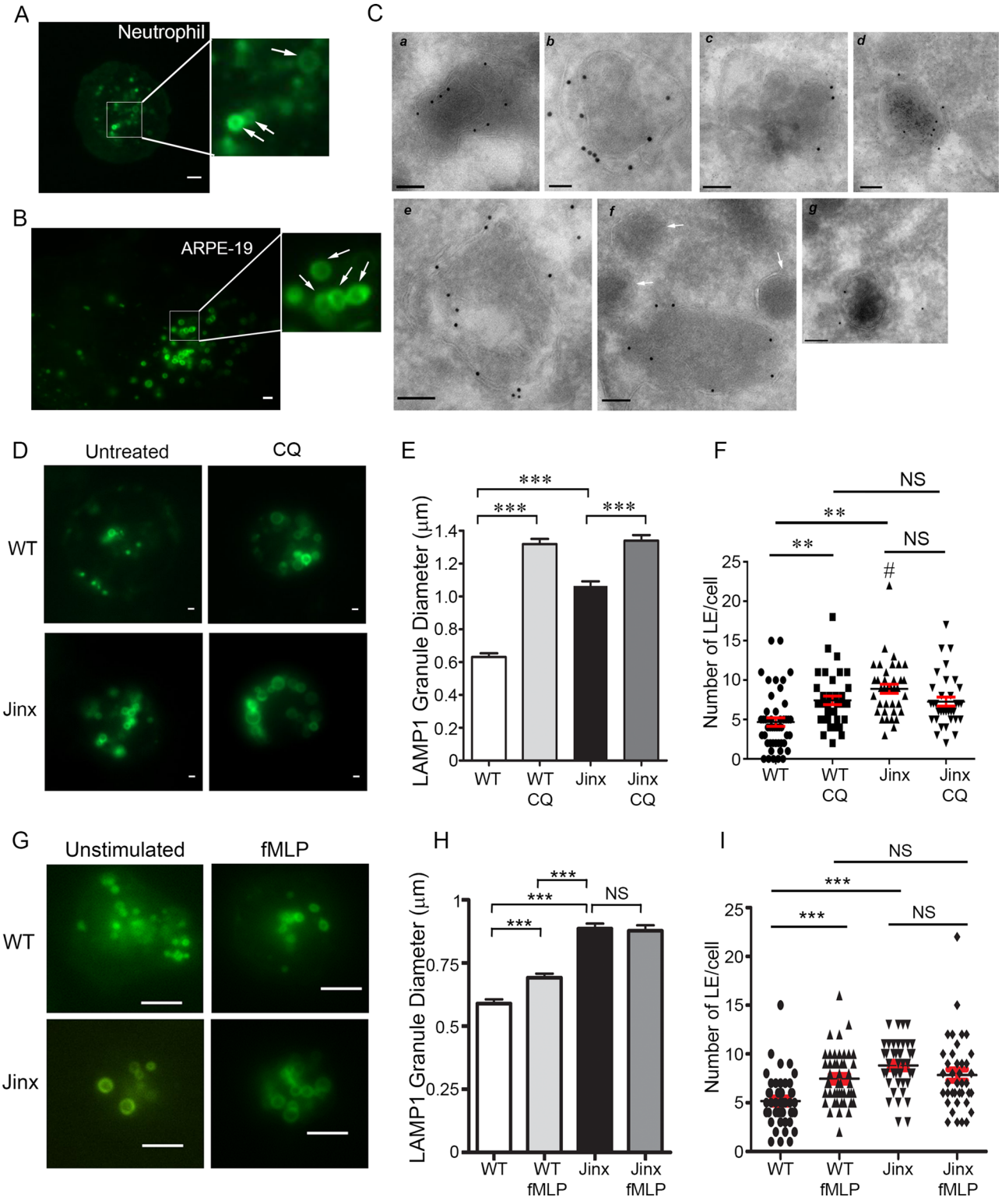

FIGURE 1: Munc13-4 regulates the size and number of LAMP1-positive late endosomes. (A, B) Representative images of TIRFM analysis of EGFP-LAMP1 in a wild-type (WT) neutrophil (A) and ARPE-19 cells (B). White arrows indicate late endosomes. Scale bar, 1 μm. For corresponding dynamic studies, see Supplemental Movies S1 and S2. (C) Representative images of immuno–electron microscopy analysis of LAMP1-positive compartments in WT (a–d) and Munc13-4-KO (e–g) neutrophils, showing LAMP1-positive multilaminar compartments (a–c and e), multivesicular bodies (f), and electron-dense smaller vesicles resembling conventional lysosomes (d, g). Unlabeled secretory organelles are indicated with arrows. Scale bars, 100 nm (a–e, g), 50 nm (f). (D) Representative images of TIRFM analyses of the distribution of EGFP-LAMP1 in primary WT or Munc13-4-KO (*Jinx*) neutrophils treated with 50 μM CQ for 4 h or vehicle. Scale bar, 1 μm. (E) Quantitative analysis of late endosomal size. Quantification was performed by measuring the diameter of EGFP-LAMP1–positive late endosomes in each cell using ImageJ. Results are mean ± SEMs. WT, WT+CQ,

live-cell fluorescence studies. Taken together, our results demonstrate that the observed distribution of LAMP1 at late endosomes in transfected neutrophils is highly specific and is in agreement with both the distribution of endogenous LAMP1 as detected by electron microscopy in this study and previous studies showing late endosomal localization of LAMP1 in these cells (Berger *et al.*, 1994). Next, to determine whether endogenous late endosomal markers could be detected at large vesicles in neutrophils, we optimized neutrophil fixation using low paraformaldehyde (PAF) concentrations to increase late endosome structure preservation. Supplemental Figure S2 shows that endogenous LAMP1 and Rab7, two markers of LEs, are detected in large vacuolar vesicles in murine neutrophils in cells fixed using low aldehyde concentration. Taken together, our data suggest that the use of EGFP-LAMP1 in transfected neutrophils is a viable and efficient method to study late endosome morphology and dynamics.

To analyze whether Munc13-4 regulates endosomal maturation, we first comparatively analyzed the size of EGFP-LAMP1–positive LEs in wild-type and Munc13-4–knockout (KO) neutrophils. In these studies, we focused on large LAMP1-positive vesicles that appeared as "hollow" vesicles in live-cell fluorescence studies. Quantitative analyses of EGFP-LAMP1 vesicle size revealed that LES are significantly enlarged in Munc13-4–deficient neutrophils, showing an average LE diameter of ~1 µm, significantly larger than those present in wild-type cells (~0.6 µm; Figure 1, D and E). Next we hypothesized that the enlarged late endosome phenotype observed in the absence of Munc13-4 was caused by the impaired fusion of late endosomes with degradative organelles, thus decreasing late endosome flux and increasing vesicle size, similar to the way in which blocking autophagosome–lysosome fusion leads to enlarged autophagosomes and substrate accumulation (Gutierrez *et al.*, 2004; Klionsky *et al.*, 2008). We then reasoned that pharmacological inhibition of late endosome–lysosome fusion should lead to a similar enlarged late endosome phenotype. To test this experimentally, we analyzed the effect of the lysosomotropic weak base chloroquine (CQ) on the size of late endosomes in neutrophils. CQ is a factor known to interfere with lysosomal pH (Tietz *et al.*, 1990) and lysosomal fusion, likely by inhibiting calmodulin-dependent mechanisms (Pryor *et al.*, 2000). Neutrophil treatment with CQ showed increased size of EGFP-LAMP1 vesicles similar to that observed in the absence of Munc13-4 (Figure 1, D and E), further suggesting a possible defect in late endosome fusion in Munc13-4 KO cells.

The up-regulation of homotypic or heterotypic late endosomal fusion may also lead to enlarged endosomal organelles, albeit generating a reduced number of organelles due to consolidation of fusing organelles into a single enlarged one. Therefore we expected that putative deficiencies in the maturation flux of late endosomes in the absence of Munc13-4 expression would result in an increased number of enlarged organelles due to the inability of the system to clear LE at an intermediate state. Quantification of the number of hollow LAMP1-positive organelles in neutrophils revealed that Munc13-4 deficiency leads to an increased number of enlarged vesicles (Figure 1F). Of importance, CQ induces an accumulation of immature LEs in wild-type cells similar to that observed in Munc13-4–KO neutrophils (Figure 1F). Taken together, our results suggest that Munc13-4 is necessary for late endosomal maturation, possibly through the regulation of tethering or fusion. However, because CQ may have additional effects on late endosomes, including swelling through osmotic effects (Poole and Ohkuma, 1981), and inhibition of acidification affects the formation of MVBs from early endosomes (Clague *et al.*, 1994) and membrane traffic out from the endosomes to the *trans*-Golgi network (Chapman and Munro, 1994), we next took a different approach that involves the stimulation of the endocytic pathway using physiological stimuli.

Thus, because the neutrophil endocytic pathway is highly up-regulated in response to the bacteria-derived formylated-peptide fMLP (Berger *et al.*, 1994), we next analyzed the effect of endocytic pathway up-regulation on endosome size. In these assays, we observed that stimulation of neutrophils with fMLP increased late endosomal size in wild-type cells. However, late endosome size was significantly further increased in Munc13-4 KO under both unstimulated and stimulated conditions. (Figure 1, G and H, and Supplemental Movies S3–S6). These results were also supported by an independent approach consisting of analyzing late endosome size in WT and Munc13-4–KO neutrophils expressing the endosomal marker Rab7, showing that Rab7-positive LEs are also enlarged in neutrophils lacking Munc13-4 (Supplemental Figure S3). Finally, wild-type cells treated with fMLP showed a significant increase in the number of LAMP1-large vesicles, whereas Munc13-4-KO cells showed a basal increased number of late endosomes that was not significantly further increased by fMLP treatment (Figure 1I). In sum, the phenotype observed in EGFP-LAMP1–expressing cells supports the idea that accumulation of enlarged LEs is induced by an intrinsic defect in Munc13-4–KO cells.

Munc13-4 interacts with syntaxin 7 in a calcium-dependent manner

Munc13-4 is proposed to mediate vesicle tethering, docking, and calcium-dependent fusion during secretion, but the molecular bases of these mechanisms are not well understood. Although previous data suggested that Munc13-4 might act as a calcium sensor for SNAREs involved in exocytosis (Boswell *et al.*, 2012), a possible role of Munc13-4 in the endocytic pathway has not been explored. To increase our understanding of the mechanisms regulated by Munc13-4 during late endosomal maturation, we analyzed the possible calcium-dependent interaction of Munc13-4 with endocytic SNARE proteins. To this end, we designed a binding assay (J.L.J. and S.D.C.) based on a lanthanide-initiated time-resolved fluorescence resonance energy transfer (TR-FRET) approach (Riddle *et al.*, 2006) to analyze Munc13-4–SNARE interactions on intracellular organelles. Munc13-4 showed significant interaction with the endocytic SNAREs syntaxin 7 and VAMP8 (Figure 2A). In addition, weak

Jinx and *Jinx*+CQ groups used 30, 40, 55, and 33 cells, respectively. ***$p < 0.0001$. (F) Quantitative analysis of the number of late endosomes in WT and *Jinx* cells treated with CQ or vehicle. Error bars are mean ± SEMs. For WT, WT+CQ, *Jinx* and *Jinx*+CQ groups, 47, 37, 37, and 34 cells were analyzed, respectively. **$p < 0.001$; #outlier; NS, not significant. (G) Representative images of TIRFM analysis of the distribution of EGFP-LAMP1 in primary WT or *Jinx* neutrophils treated with 10 µM fMLP or vehicle. Scale bar, 5 µm. For the corresponding dynamic studies, see Supplemental Movies S3–S6. (H) Quantitative analysis of late endosomal size. Quantification was performed by measuring the diameter of EGFP-LAMP1–positive late endosomes in each neutrophil using ImageJ. Results are mean ± SEMs. WT, WT fMLP, *Jin*, and *Jinx* fMLP groups used 51, 73, 71, and 48 cells, respectively. ***$p < 0.0001$; NS, not significant. (I) Quantitative analysis of the number of late endosomes in WT and *Jinx* neutrophils treated with fMLP or vehicle. Error bars are mean ± SEMs. In WT, WT fMLP, *Jinx*, and *Jinx* fMLP groups, 50, 48, 45, and 40 cells were analyzed, respectively. ***$p < 0.0001$; NS, not significant.

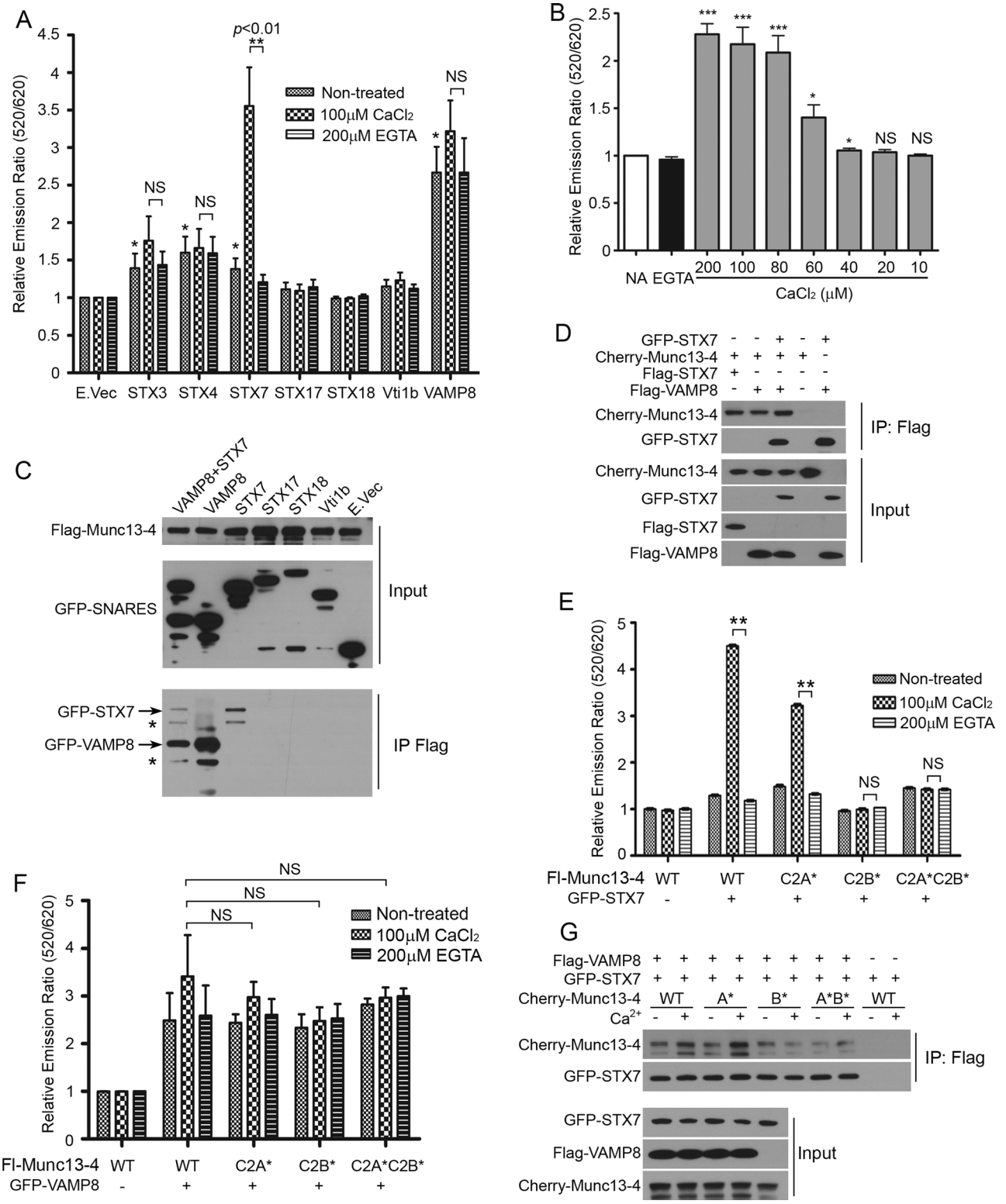

FIGURE 2: Munc13-4 binds to syntaxin 7 and VAMP8 in a calcium-dependent manner. (A) Binding assays for Munc13-4 and SNARE proteins. The binding of Flag-Munc13-4 to several GFP-tagged SNARE proteins or GFP (E. Vec) was analyzed by the TR-FRET assay as described in *Materials and Methods*. The reactions were carried out using 293T cell lysates. Where indicated, the reactions were performed in the presence of 100 μM $CaCl_2$ or 200 μM EGTA. Triplicates of one experiment, representative of at least four experiments. *$p < 0.05$; NS, not significant. STX, syntaxin. (B) Binding assays of Munc13-4 and syntaxin 7 in the presence of 100 μM EGTA or $CaCl_2$ at the indicated total calcium concentration. Emission ratios were normalized to sample NA (no addition). The results are expressed as mean ± SEM. NS, not significant. ***$p < 0.001$ and *$p < 0.05$ vs. EGTA. (C, D) Coimmunoprecipitation assays were carried out using anti-Flag beads and 293T cell lysates expressing the indicated proteins. The cells were disrupted by nitrogen cavitation in either relaxation buffer (C) or RIPA buffer (D) as described in *Materials and Methods*. Western blots are representative

but significant binding to syntaxin 3 and syntaxin 4 was observed. However, Munc13-4 did not show specific binding to syntaxin 17, syntaxin 18, or the endocytic protein vesicle transport through interaction with t-SNAREs 1B (Vti1b; Figure 2A). Munc13-4 binding to syntaxin 7 but not to VAMP8 was significantly increased in the presence of calcium (Figure 2A). However, Munc13-4 binding to other syntaxins, including syntaxin 3 and syntaxin 4, was only marginally increased by the divalent cation. Dose–response assays show that binding increases significantly in the presence of calcium down to a total calcium concentration of 40 µM (Figure 2B), which is similar to the half-maximal effective concentration (EC_{50}) calcium dependence of ~23 µM previously found for Munc13-4 stimulation of liposome fusion (Boswell *et al.*, 2012). Because calcium-dependent mechanisms regulate multiple aspects of vesicular fusion, we considered the calcium-dependent binding to syntaxin 7 to be physiologically relevant and therefore studied this interaction in further detail.

Using an independent approach consisting of coimmunoprecipitation (CoIP) assays of tagged proteins, we confirmed that Munc13-4 is able to pull down both syntaxin 7 and VAMP8 either independently or when coexisting in the same lysates (Figure 2C). In these assays, we showed that syntaxin 7 and VAMP8 but no other syntaxins or Vti1b coimmunoprecipitate with Flag–Munc13-4 but not with anti-Flag beads (Figure 2C), confirming that the binding is specific. Furthermore, counter-immunoprecipitation assays confirmed that syntaxin 7 and VAMP8 are able to pull down mCherry–Munc13-4 (Figure 2D). Finally, VAMP8 was able to coimmunoprecipitate both Munc13-4 and syntaxin 7 when coexpressed in the same lysates, suggesting that the three proteins might form a tripartite complex (Figure 2D).

Munc13-4 C2 domains conserve five aspartic acids, which are known to coordinate calcium binding in other C2 domains (Feldmann *et al.*, 2003). As a consequence, both Munc13-4 C2 domains regulate calcium-dependent mechanisms (Boswell *et al.*, 2012), and Munc13-4 enhances Ca^{2+}-induced secretion (Shirakawa *et al.*, 2004). To determine whether the Ca^{2+}-binding sites in Munc13-4 are necessary to mediate binding to syntaxin 7 and determine the molecular basis of the syntaxin 7–Munc13-4 interaction, we mutated the aspartic acids D127 and D133 to alanines in loop 1 of the Munc13-4 C2A domain, which forms calcium binding sites 1, 2, and 4 (Rizo and Sudhof, 1998; Feldmann *et al.*, 2003). Next we mutated residues D941 and D947 to knock out the Ca^{2+}-binding site in loop 1 of the C2B domain. Mutation of aspartic acid residues to alanine in either the C2B domain or in both C2A and C2B domains, but not in the C2A domain only, markedly decreased the affinity of Munc13-4 for syntaxin 7 (Figure 2E) but not for VAMP8 (Figure 2F), indicating that the C2B domain is essential for the Munc13-4–syntaxyn7 interaction.

Munc13-4 coimmunoprecipitates with syntaxin 7 and VAMP8 in a calcium-dependent manner

To analyze whether Munc13-4 forms a complex with both SNARE proteins, we carried out CoIP assays using lysates from cells expressing Flag-VAMP8, GFP–syntaxin 7, and mCherry–Munc13-4. We found that both syntaxin 7 and Munc13-4 coimmunoprecipitate with VAMP8 (Figure 2, D and G). Of interest, CoIP of Munc13-4 but not syntaxin 7 with VAMP8 was up-regulated by the presence of calcium, as manifested by increased levels of Munc13-4 detected in the pull-down pellet. Furthermore, the calcium-dependent CoIP of Munc13-4 with the syntaxin 7/VAMP8 complex was partially inhibited by mutation of the calcium-binding sites in either the C2B or the C2A-C2B domains but not in the C2A domain alone (Figure 2G), further supporting a role for Munc13-4–C2B in calcium-dependent binding to the SNARE complex through syntaxin 7 and a calcium-independent binding through VAMP8. These results, together with those obtained using the binding assay (Figure 2, A and E), suggest that Munc13-4, syntaxin 7, and VAMP8 form a dynamic complex and that the binding of Munc13-4 to syntaxin 7 is susceptible to calcium-mediated regulation.

Munc13-4 and syntaxin 7 colocalize at late endosomes

In neutrophils, LAMP1 localizes exclusively at late endosomes (Cieutat *et al.*, 1998) but not at the azurophilic granules, which are members of the lysosome-related organelle family (Dell'Angelica *et al.*, 2000) and are characterized by the presence of LAMP3 and an array of proteases and secretory proteins, including myeloperoxidase (Kuijpers *et al.*, 1991). Therefore, to analyze the localization of syntaxin 7 and Munc13-4 at late endosomes, we studied the distribution of endogenous syntaxin 7 and Munc13-4 in relationship to that of LAMP1 by immunofluorescence in primary neutrophils. Of importance, although 4% PAF may induce shrinkage and deformation of late endosomes, probably as a result of the hyperosmolarity property of the fixative and dehydration of the sample (Murk *et al.*, 2003), morphological changes occur without affecting the membrane length (Murk *et al.*, 2003) or protein localization, and therefore its use is valid for colocalization analyses. In Figure 3A, we show that syntaxin 7 and Munc13-4 colocalize at LAMP1-positive structures in these cells. As described previously, Munc13-4 was also detected at lysosome-related organelles in neutrophils, where it also colocalizes with syntaxin 7 (Figure 3B). Quantitative analysis showed that 33% of LAMP1-positive vesicles contain Munc13-4 and 39% of LEs contain syntaxin 7, confirming the distribution of Munc13-4 at LEs (Figure 3C). Next we studied the localization of Munc13-4 and syntaxin 7 in further detail using high-resolution single-molecule fluorescence microscopy (STORM). As shown in Figure 3D, our studies demonstrate adjacent distribution of syntaxin 7 and Munc13-4 within 20–50 nm in the lateral plane, suggesting that they are likely to interact in vivo. We also observed a similar pattern for LAMP1 and Munc13-4, which appeared in close proximity, although in most cases, these two molecules are separated from each other (>50 nm; Figure 3E), suggesting a high likelihood of occupying the same organelle but not necessarily being adjacent and thus unlikely to interact.

Because Munc13-4 and syntaxin 7 are expressed in several cells and tissues (Wang *et al.*, 1997; Koch *et al.*, 2000), we confirmed their cellular colocalization in human retinal pigment epithelial cells (ARPE19 cells). To this end, we analyzed the localization of Munc13-4 in relation to that of syntaxin 7 by pTIRFM in live cells, which has the advantage of allowing the analysis of deeper cellular structures than traditional TIRFM while maintaining a high signal-to-background ratio and low photobleaching (Mudrakola *et al.*, 2009). Figure 3F shows that Munc13-4 largely colocalizes with syntaxin 7 at both the

of at least three experiments with similar results. The asterisk indicates truncations. (E, F) Analysis of the binding of Munc13-4 WT or mutants C2A*, C2B*, and C2A*C2B* to syntaxin 7 (E) or VAMP8 (F). C2A* includes point mutations D127 and D133 to alanines in the Munc13-4 C2A domain, which knocks out the Ca^{2+}-binding sites in this domain; C2B* includes point mutations D941 and D947 to alanines to knock out the Ca^{2+}-binding sites in the C2B domain. C2A*C2B* includes four D → A mutations corresponding to both C2 domains. NS, not significant. $^{**}p < 0.001$. (G) Coimmunoprecipitation assays were performed as in C, except that reactions were performed in the presence or absence of 100 µM calcium (Ca^{2+}), and, where indicated, Munc13-4 C2 mutants were used instead of WT Munc13-4.

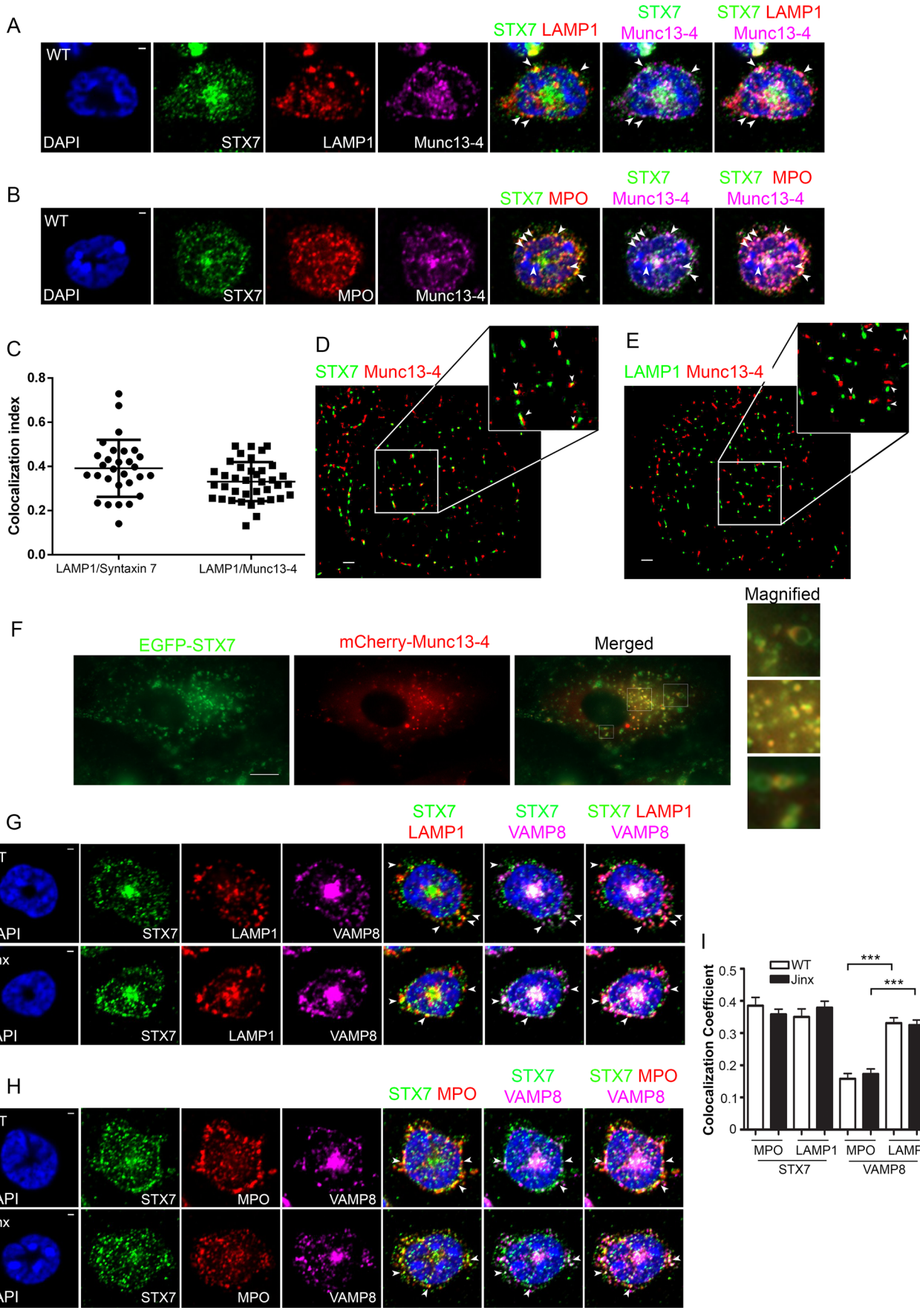
A
WT
DAPI
STX7
LAMP1
Munc13-4
STX7 LAMP1
STX7 Munc13-4
STX7 LAMP1 Munc13-4
B
WT
DAPI
STX7
MPO
Munc13-4
STX7 MPO
STX7 Munc13-4
STX7 MPO Munc13-4
C
Colocalization index
0.8
0.6
0.4
0.2
0.0
LAMP1/Syntaxin 7
LAMP1/Munc13-4
D
STX7 Munc13-4
E
LAMP1 Munc13-4
F
EGFP-STX7
mCherry-Munc13-4
Merged
Magnified
G
WT
DAPI
STX7
LAMP1
VAMP8
Jinx
STX7 LAMP1
STX7 VAMP8
STX7 LAMP1 VAMP8
H
WT
DAPI
STX7
MPO
VAMP8
Jinx
STX7 MPO
STX7 VAMP8
STX7 MPO VAMP8
I
Colocalization Coefficient
0.5
0.4
0.3
0.2
0.1
0
WT
Jinx
***
***
MPO
LAMP1
MPO
LAMP1
STX7
VAMP8

limiting membrane of hollow vesicles and at the membranes of small vesicles (Pearson $r = 0.755$, $n = 16$).

The distribution of syntaxin 7 at late endosomes is independent of Munc13-4

To analyze whether Munc13-4 is necessary for the subcellular distribution of syntaxin 7, we carried out immunofluorescence analysis of endogenous syntaxin 7 in Munc13-4–deficient neutrophils. In Figure 3, G and I, we show that the percentage of total syntaxin 7 present in late endosomes of Munc13-4–deficient cells is not significantly different from that detected in wild- type cells, indicating that the distribution of syntaxin 7 at late endosomes is independent of Munc13-4 expression. Similar results were also observed for VAMP8. Thus ~35% of LAMP1-positive late endosomes expressed VAMP8 in neutrophils independently of the expression of Munc13-4.

A previous study suggested that although both VAMP8 and syntaxin 7 are localized at late endosomes, the general distribution of VAMP8 does not necessarily mirror that of syntaxin 7 (Mullock *et al.*, 2000). To test this in neutrophils, and because Munc13-4 localizes not only at late endosomes but also at azurophilic granules (Catz, 2013), we analyzed the distribution of VAMP8 and syntaxin 7 at this set of granules. Immunofluorescence studies show that whereas ~40% of azurophilic granules contain syntaxin 7 in wild-type and Munc13-4–KO neutrophils, only ~15% of MPO-positive granules express VAMP8 (Figure 3, H and I). These data suggest that the distribution of the SNAREs VAMP8 and syntaxin 7 is independent of Munc13-4 expression, and, in agreement with results in Madin–Darby canine kidney cells (Mullock *et al.*, 2000), VAMP8 and syntaxin 7 are not equally distributed in neutrophils. Thus it is possible that azurophilic granules lacking VAMP8 may constitute a subpopulation of lysosome-related organelles at a different maturation stage or may use a different SNARE complex.

Next we confirmed the dual distribution of syntaxin 7 at both secretory granules and late endosomes in neutrophils expressing EGFP–syntaxin 7 using pTIRFM. This analysis showed that syntaxin 7 localizes at a highly dynamic set of punctate vesicles, as well as at late endosomes identified by their hollow appearance in live-cell microscopy similar to those with LAMP1 expression (Supplemental Figure S4A and Supplemental Movie S7). A different pattern of protein distribution was observed for syntaxins 3 and 4, which were localized at punctate vesicular structures and the neutrophil plasma membrane but not LEs (Supplemental Figure S4, B and C), in agreement with a previous study (Brumell *et al.*, 1995). Finally, the distribution of Munc13-4 in live neutrophils was similar to that observed for syntaxin 7, with the protein split between highly dynamic secretory vesicles and late endosomes (Supplemental Figure S4D).

Munc13-4 expression but not the syntaxin 7 calcium-binding–deficient mutant Munc13-4 C2A*C2B* rescues the enlarged late endosomal phenotype

To demonstrate that calcium-dependent binding of Munc13-4 to syntaxin 7 regulates endosomal maturation, we transfected Munc13-4–deficient neutrophils with either Munc13-4 or Munc13-4-C2A*C2B*, a mutant of Munc13-4 that disrupts this interaction (Figure 4A). Here we show that wild-type Munc13-4 but not the double C2–domain mutant rescues the normal late endosomal size in neutrophils (Figure 4B), further supporting the finding that Munc13-4 regulates late endosomal maturation through a mechanism that involves the participation of the calcium-binding properties of this molecule, most likely through interaction with syntaxin 7.

Intraluminal acidity is not regulated by Munc13-4

Intraluminal acidity is essential for LEs and lysosomes to become biologically active degradative compartments (Huotari and Helenius, 2011). We next analyzed whether Munc13-4 regulates LE acidity. To this end, we double labeled LEs with the limiting membrane marker EGFP-LAMP1 and the acidotropic probe LysoTracker. Figure 5A and associated Supplemental Movies S8 and S9 show that LysoTracker-positive LEs are similarly present in both WT and Munc13-4–KO neutrophils. No significant differences were observed in the total number of acidic organelles between wild-type and Munc13-4–KO cells as determined by the number of LysoTracker-labeled enlarged EGFP-LAMP1 LEs (Figure 5B). Taken together, our results rule out a significant role for Munc13-4 in the regulation of the pH of LEs.

Munc13-4 is required for CpG-ODN–dependent endosome maturation and TLR9-dependent signaling

Endosome maturation is a requirement for endosomal-initiated signaling in response to several stimuli, including the stimulation of the pattern recognition receptor TLR9 by unmethylated bacterial DNA (Hacker *et al.*, 1998). Here, to further evaluate the role of Munc13-4 in endosomal maturation and function, we analyzed the distribution of TLR9 in relation to the subcellular localization of Munc13-4. Immunofluorescence analysis of endogenous proteins showed the localization of TLR9 at Munc13-4–positive intracellular compartments (Figure 6A); 33.3 ± 2.3% of TLR9 compartments contain Munc13-4 ($n = 57$ cells). In addition, TLR9 was detected in compartments that were positive for the endosomal markers LAMP1 (28.36 ± 1.96% of LAMP1 compartments contain TLR9; $n = 40$) and syntaxin 7 (54.89 ± 2.5% of TLR9 compartments contain syntaxin 7; $n = 37$; Figure 6A). Because TLR9 activation requires endosomal maturation, we next analyzed the distribution of the unmethylated

FIGURE 3: Syntaxin 7 and Munc13-4 colocalize in LAMP1-positive granules in neutrophils, but the subcellular localization of syntaxin 7 and VAMP8 is independent of Munc13-4. (A) Immunofluorescence analysis of endogenous syntaxin 7 (STX7; green), the late endosomal marker LAMP1 (red), and Munc13-4 (violet) in wild-type neutrophils. Arrowheads indicate examples of vesicles that are positive for all three stainings. Cell nuclei were visualized with 4′,6-diamidino-2-phenylindole (DAPI) staining (blue). (B) Immunofluorescence analysis of endogenous syntaxin 7 (green), the lysosome-related organelle marker MPO (red), and Munc13-4 (violet) in wild-type neutrophils. (C) Colocalization analysis of LAMP1 with either syntaxin 7 or Munc13-4 using 29 and 38 cells, respectively. (D, E) High-resolution STORM analysis of the localization of endogenous Munc13-4 and syntaxin 7 (D) or LAMP1 (E) in wild-type cells. Whereas syntaxin 7 and Munc13-4 are detected adjacent to each other (arrowheads, 10–50 nm; D), LAMP1 and Munc13-4 are in close proximity but not always adjacent (arrowheads, estimated distance >50 nm; E). Scale bar, 1 µm. (F) TIRFM analysis of colocalization of syntaxin 7 and Munc13-4 in RPE cells. Scale bar, 10 µm. (G, H) Immunofluorescence analyses of endogenous syntaxin 7 (green) and VAMP8 (violet) with LAMP1 (red; G) or MPO (red; H) in wild-type and Munc13-4–KO neutrophils. Arrowheads indicate examples of vesicles that are positive for all three stainings. Scale bar, 1 µm. (I) Quantification of the colocalization shown in G and H. Calculation of the colocalization coefficient was performed by analyzing at least 38 cells in each group. Results are mean ± SEM. ***$p < 0.001$.

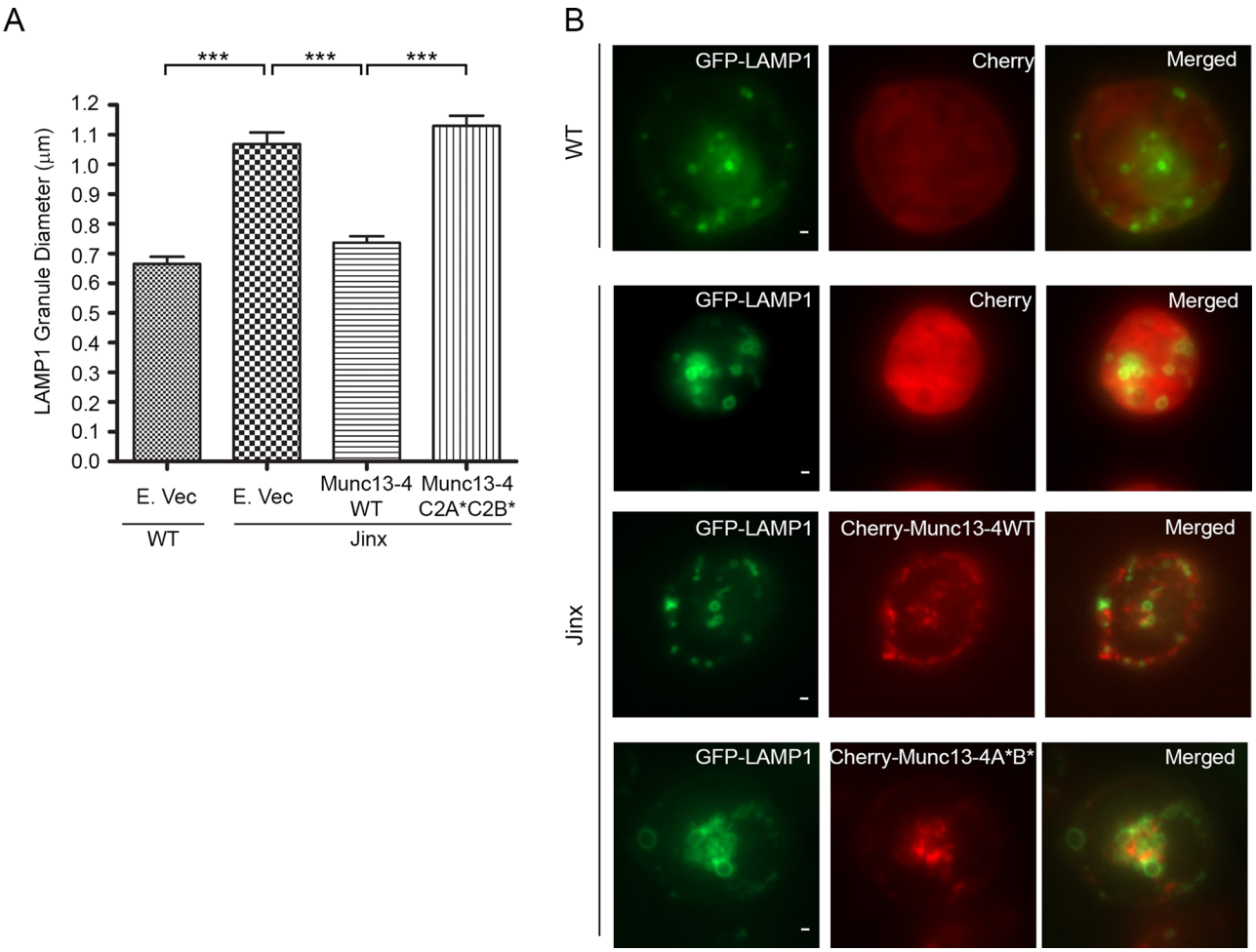

FIGURE 4: Munc13-4 wild type but not the syntaxin 7 binding–deficient mutant Munc13-4 C2A*C2B* rescues the late endosome enlargement phenotype in Munc13-4–KO cells. (A) WT and Munc13-4–KO (*Jinx*) neutrophils were cotransfected with EGFP-LAMP1 and mCherry-Munc13-4 wild type (Munc13-4 WT), mCherry-Munc13-4 C2A*C2B* mutant (Munc13-4C2A*C2B*), or mCherry empty vector (E. Vec). Quantification of EGFP-LAMP1–positive late endosome diameters was performed as in Figure 1. Results are mean ± SEMs, with 40, 47, 32, and 42 cells quantified for groups WT with mCherry empty vector, *Jinx* with mCherry empty vector, *Jinx* with mCherry-Munc13-4-WT, and *Jinx* with mCherry-Munc13-4-C2A*C2B* mutant, respectively. ***$p < 0.0001$. (B) Representative TIRFM images of cells from A. Cells were imaged 6 h after nucleofection. Scale bar, 1 μm.

DNA receptor in relation to cathepsin G, a protease previously associated with lysosome-related organelles in neutrophils (Egesten *et al.*, 1994) that is also present in a subpopulation of LAMP1-positive puncta in murine neutrophils (Supplemental Figure S5). Because the colocalization of LAMP1 with the lysosome-related organelle marker myeloperoxidase is very poor (unpublished data), we propose that cathepsin G colocalizes with LAMP1 at organelles that correspond to conventional lysosomes in these cells (also observed by LAMP1 staining and electrodensity, by immuno–electron microscopy, in Figure 1). We found that neutrophils lacking Munc13-4 showed decreased colocalization of late endosomal TLR9 with lysosomal cathepsin G both under unstimulated conditions and after treatment with the unmethylated oligonucleotide CpG-ODN, a well-characterized TLR9 agonist (Figure 6, B and C). In addition, whereas wild-type cells showed a significant increase in TLR9–cathepsin G colocalization in response to CpG, no significant effect was observed in Munc13-4–deficient cells, further supporting a role for Munc13-4 in the maturation of the TLR9-positive compartment (Figure 6, B and C).

To characterize further the nature of EGFP-LAMP1–positive late endosomes and determine their degradative capacity, we used DQ-BSA, an endocytic substrate that becomes fluorescent upon digestion of BSA and subsequent release of the unquenched fluorescent probe. Our data show that some of the LAMP1-positive large vesicles function as degradative compartments (Figure 6D). Furthermore, quantitative analyses by two independent methods (confocal microscopy and flow cytometry) show decreased degradative capacity in Munc13-4–KO cells compared with wild-type cells, further supporting a retarded or defective delivery of degradative enzymes into LEs in the absence of Munc13-4 expression.

Next, to study a possible regulatory function for Munc13-4 on late endosomal–initiated TLR9 signaling, we analyzed the signaling pathways initiated by CpG-ODN in primary neutrophils. Wild-type neutrophils stimulated with CpG-ODN 1826 showed a marked and transient increase in extracellular signal regulated kinase (ERK) phosphorylation (Figure 6E). ERK phosphorylation peaked at 10 min and gradually decayed but still showed signs of activation up to 40 min after the addition of CpG (Figure 6, E and F). In contrast, Munc13-4–deficient

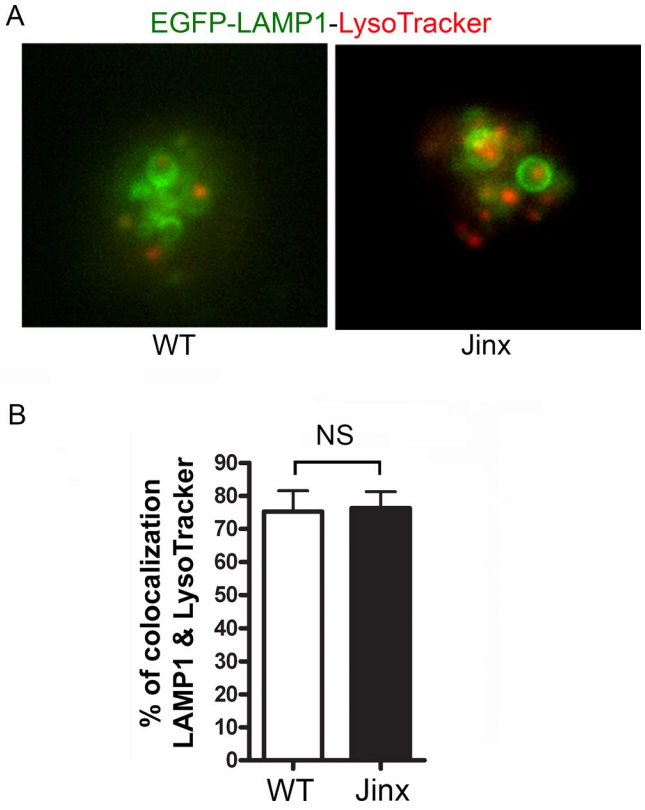

FIGURE 5: Intraluminal acidity is not regulated by Munc13-4. (A) Representative images of TIRFM analyses of the distribution of EGFP-LAMP1 and acidic organelles (LysoTracker) in primary WT or Munc13-4-KO (*Jinx*) neutrophils. For the corresponding dynamic studies, see Supplemental Movies S8 and S9. (B) Quantitative analysis of the colocalization of LAMP1 and LysoTracker in unstimulated neutrophils. Results are expressed as mean ± SEM from 18 WT and 17 Munc13-4–KO cells from two independent experiments.

neutrophils showed a weak ERK phosphorylation response to CpG that was significantly different from the response observed in wild-type cells (Figure 6, E and F). No differences were observed between wild-type and Munc13-4–KO neutrophils in levels of p38MAP kinase phosphorylation in response to TLR9 activation (Figure 6E), supporting a Munc13-4–dependent Erk-specific activation mechanism in neutrophils stimulated with CpG. Furthermore, no differences were observed in the level of expression of TLR9 between wild-type and Munc13-4–deficient neutrophils (Figure 6G), indicating that the defects are not due to an intrinsic deficiency in TLR9.

Munc13-4 is required for endosomal-initiated, TLR9-dependent neutrophil activation

The results showing that late endosome–initiated signaling is impaired in Munc13-4–deficient neutrophils suggested that this protein may play an important role in the regulation of several cellular functions downstream of TLR9 activation. CD11b up-regulation is a process of fundamental importance in innate immunity, as it controls the ability of neutrophils to adhere to the activated endothelium during infections (Moreland *et al.*, 2002) and mediates host–pathogen recognition (Forsyth *et al.*, 1998). Here, to study the role of Munc13-4 in the activation of endosomal TLR9-associated functions, we next analyzed the plasma membrane up-regulation of the β_2-integrin subunit CD11b in response to CpG in wild-type and Munc13-4–deficient neutrophils. Murine neutrophils stimulated with CpG showed marked up-regulation of CD11b at the plasma membrane (Figure 7, A and B). The process was inhibited by pretreatment of neutrophils with chloroquine, indicating that a fully functional endosomal system is necessary for CpG to induce CD11b up-regulation (Figure 7, A and B). Furthermore, β_2-integrin activation by CpG was significantly impaired in Munc13-4–KO neutrophils, further supporting a role for Munc13-4 in endosomal-initiated, TLR9-dependent neutrophil activation (Figure 7, A and B). Of note, CD11b up-regulation during neutrophil activation is an otherwise Munc13-4–independent mechanism, as neutrophils lacking Munc13-4 are able to activate β_2-integrins at the plasma membrane in response to other physiological stimuli that do not signal from the late endosomal compartment. This includes the bacterial-derived peptide fMLP (Figure 7, C and D) and the TLR4 ligand lipopolysaccharide (Johnson *et al.*, 2011). In addition, the up-regulation of CD11b by fMLP was not affected by CQ, further supporting the idea that the effect of this weak base is specific for stimuli that depend on the proper function of the endocytic compartment (Figure 7, C and D). Finally, to consolidate the data from signaling studies with the functional results, we analyzed whether the defects observed in TLR9-initiated Erk signaling were associated with the impaired ability of Munc13-4–KO neutrophils to mediate CD11b up-regulation. Here we show that Erk phosphorylation and CD11b up-regulation in response to TLR9 agonists are inhibited by PD98059, a well-characterized ERK inhibitor (Figure 7, E and F, respectively). The effect was not observed in Munc13-4–KO cells with an already low intrinsic response to CpG, thus functionally connecting Munc13-4 function, ERK signaling, and CD11b up-regulation in response to TLR9 agonists. Taken together, our data strongly support an important role for Munc13-4 in late endosomal maturation that is associated with the regulation of signaling processes and cellular functions of fundamental importance in biological processes.

DISCUSSION

In this work, we characterized a novel mechanism of late endosomal maturation regulated by Munc13-4 that has direct implications for signaling pathways regulating cellular functions associated with the immune response. Here we identified Munc13-4, a trafficking protein previously associated with secretory mechanisms, as a central regulatory component of the endocytic pathway. In particular, we established that Munc13-4 binds to the SNAREs syntaxin 7 and VAMP8, identified the molecular determinants of these interactions, and showed that cells deficient in Munc13-4 are associated with several late endosomal defects, including impaired LE maturation and impaired TLR9-dependent activation, which cannot be rescued by mutants of Munc13-4 that lack the calcium-dependent SNARE-binding properties.

In recent years, several studies have made progress in helping to clarify the mechanism of late endosomal fusion events. These studies identified the HOPS complex and Rab7 as tethering factors (Caplan *et al.*, 2001; Solinger and Spang, 2013) and syntaxin 7, VAMP7, and VAMP8 as essential SNAREs for regulated fusion (Luzio *et al.*, 2007). Furthermore, the participation of intraluminal calcium in the prefusion events of late endosomes and lysosomes was demonstrated (Pryor *et al.*, 2000). This suggested that a calcium sensor may mediate this process, similar to the mechanism used by synaptotagmin VII during lysosomal fusion with the plasma membrane. However, based on the inhibitory effect of high calcium concentrations on LE–lysosomal fusion, it was indicated that synaptotagmin VII does not regulate LE fusion (Luzio *et al.*, 2010), suggesting that a sensor for LE–lysosome fusion is yet to be identified. Munc13-4 has the ability to regulate vesicular trafficking, docking, and fusion in a

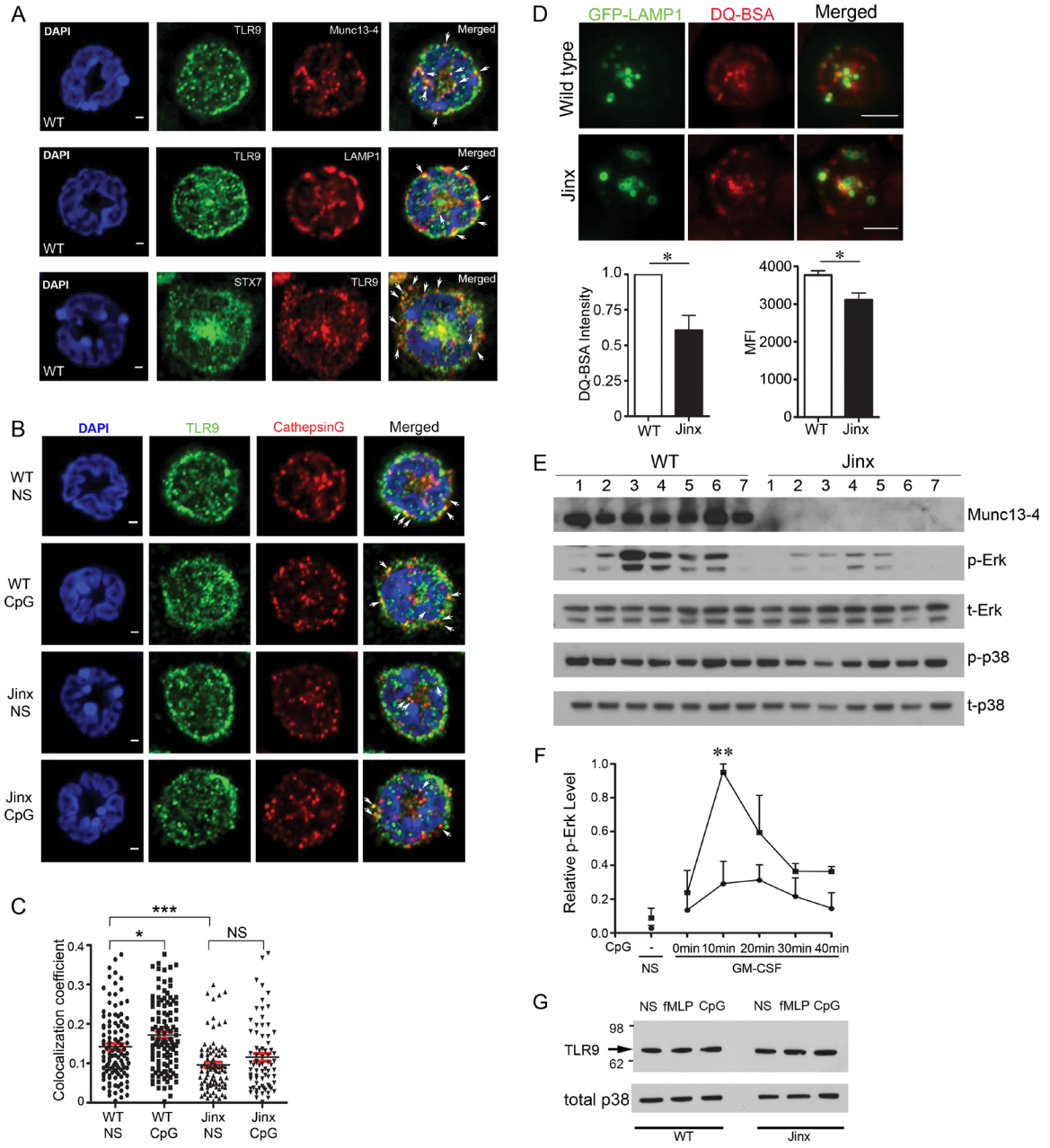

FIGURE 6: Munc13-4 is required for CpG-ODN–induced endosomal maturation and TLR9-dependent signaling. (A) Confocal microscopy analysis of the distribution of TLR9 with Munc13-4, LAMP1, and STX7 in WT neutrophils. Cell nuclei are visualized with DAPI staining (blue). Scale bar, 1 μm. (B) Confocal microscopy analysis of the distribution of TLR9 with the protease cathepsin G in WT and Munc13-4–KO (*Jinx*) neutrophils. NS, no stimulation; CpG, cells were primed with GM-CSF and treated with CPG-ODN. Scale bar, 1 μm. (C) Quantification analysis showing the percentage of TLR9-positive vesicles that contain cathepsin G. In these assays, 109, 113, 131, and 137 cells were analyzed for the groups WT NS, WT+CpG, *Jinx* NS, and *Jinx*+CpG, respectively. Results are expressed mean ± SEM. *$p < 0.05$, ***$p < 0.0001$. (D) Top, pTIRFM images of WT and *Jinx* neutrophils expressing GFP-LAMP1 (green) with internalized DQ-BSA (red), a fluorescent probe whose intensity increases upon degradation. The fluorescence intensity of the probe was analyzed from confocal images using ImageJ (bottom left) or by flow cytometry (bottom right). Results are mean ± SEMs. For the quantification of confocal images, 342 WT and 344 *Jinx* neutrophils were analyzed. For flow cytometry, $n = 3$ for both WT and Jinx. *$p < 0.05$. (E) Western blot analysis of neutrophil signaling in response to TLR9 activation. WT and Munc13-4–KO (*Jinx*) neutrophils were treated as follows: 1, untreated; 2, GM-CSF 1.5 h; 3, GM-CSF 1.5 h + CpG 10 min; 4, GM-CSF 1.5 h + CpG 20 min; 5, GM-CSF 1.5 h + CpG 30 min; 6, GM-CSF 1.5 h + CpG 40 min; and 7, CpG 10 min. Immunoblots are representative of three independent experiments. (F) Quantification of Erk phosphorylation upon GM-CSF and CpG treatment was performed by densitometry. The intensity of phosphorylated Erk was normalized to that of total Erk, and then all the relative intensity values were normalized to the highest value (WT GM-CSF 1.5 h + CpG 10 min). Squares indicate WT and circles indicate *Jinx* neutrophils. The results are presented as mean ± SEM ($n = 3$); **$p < 0.005$. (G) TLR9 expression in WT and Munc13-4–KO neutrophils. Total p38 was used for equal loading. NS, no stimulation.

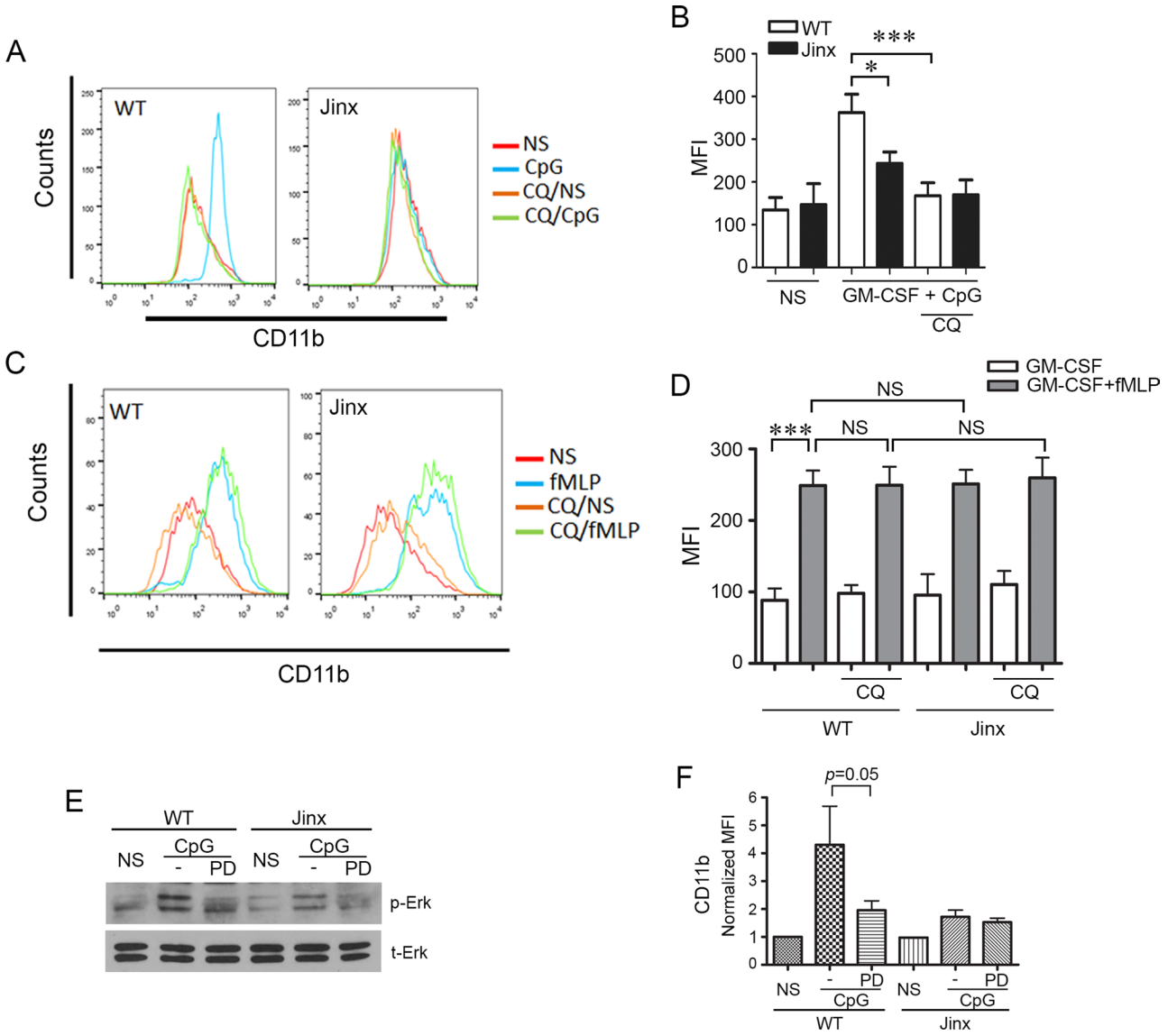

FIGURE 7: TLR9-induced plasma membrane up-regulation of CD11b is impaired in Munc13-4–KO neutrophils. (A) Flow cytometry analysis of the up-regulation of CD11b at the plasma membrane of WT or Munc13-4–KO (*Jinx*) neutrophils. Where indicated, the cells were treated with CQ or vehicle before stimulation with the unmethylated oligonucleotide CpG-ODN. (B) Quantitative analysis of the effect of CpG and chloroquine on CD11b up-regulation in WT and *Jinx* neutrophils primed with GM-CSF. Mean ± SEM. $n = 10$; ***$p < 0.001$, *$p < 0.02$. (C, D) Flow cytometry analysis and quantification of the up-regulation of CD11b at the plasma membrane in WT or Munc13-4–KO neutrophils stimulated with fMLP and/or GM-CSF. Where indicated, the cells were preincubated in the presence of CQ before stimulation. Mean ± SEM. $n = 10$; ***$p < 0.001$. (E) Effect of the inhibitor PD98059 (PD) on Erk phosphorylation. (F) Effect of the inhibitor PD on CD11b up-regulation. Mean ± SEM of three independent experiments.

calcium-dependent manner. Our data show that Munc13-4 interacts with VAMP8 and syntaxin 7 and that the interaction is favored in the presence of calcium. They also show that mutations in the calcium-binding domain of Munc13-4 impair binding to syntaxin 7. This supports the idea that Munc13-4 may operate as a calcium sensor for LE fusion.

Munc13-4 was shown to reconstitute calcium-dependent, SNARE-mediated membrane fusion in vitro, albeit in association with the secretory syntaxins 1, 3, and 4 instead of endosomal syntaxins (Boswell *et al.*, 2012). That study demonstrated that whereas both C2 domains of Munc13-4 were important for calcium-dependent fusion, the Munc13-4 C2A domain but not the C2B domain was important for binding to the secretory SNARE syntaxin 1 in pull-down assays, using syntaxin-containing phosphatidylcholine liposomes (Boswell *et al.*, 2012). In principle, this differs from our observation that mutations in the C2B but not in the C2-calcium-binding domain impairs binding to syntaxin 7. Although several different possible scenarios might help to explain these differences, the most likely explanation is that syntaxins 1, 3, and 4 are significantly different proteins from syntaxin 7, with very low or no primary structure homology between secretory and endocytic syntaxins (Teng *et al.*, 2001). Therefore it is likely that Munc13-4 has evolved to recognize and interact with functionally different syntaxins through distinct C2 domains. Thus it is possible that Munc13-4 uses different C2 domains to bind to SNAREs that mediate different but complementary cellular functions, allowing a

possible sequential regulatory function. For example, Munc13-4 could serve as a regulator for both late endosomal maturation and secretion by binding simultaneously to different syntaxins.

Consistent with a possible role for Munc13-4 in LE maturation, here we show that Munc13-4–deficient cells are characterized by the presence of enlarged LAMP1-positive LEs. Although the formation of highly enlarged LEs has been demonstrated in response to the up-regulation of the endocytic pathway in other work, for example, by the up-regulation of Rab7 (Bucci *et al.*, 2000) or Rab11 activation (Savina *et al.*, 2005), these mechanisms are accompanied by an overall decreased number of enlarged vesicles due to the merging of several LE endosomes into newly formed hybrid vesicles. In fact, the formation of giant LEs was impaired by inhibiting fusion by means of calcium chelators, leading to the formation of numerous vesicles with a typical ring-shaped structure (Savina *et al.*, 2005). In our studies, the phenotype observed in Munc13-4–KO cells was characterized by a significant increase in both the size and number of LEs, which was most likely associated with the disruption of the LE flux, in the same manner that inhibition of fusion of LE (Savina *et al.*, 2005) or autophagosomes (Gutierrez *et al.*, 2004; Klionsky *et al.*, 2008) with lysosomes increases the number of LEs or LC3-positive organelles, respectively. Supporting this view, treatment of wild-type cells with chloroquine, a base that inhibits fusion of endocytic vesicles with lysosomes (Pryor *et al.*, 2000), reproduced the large-LE phenotype observed in Munc13-4–deficient cells and increased the number of LEs to levels similar to those present in Munc13-4–KO cells (Figure 1, D and E). Furthermore, rescue experiments with Munc13-4 demonstrated that this protein is necessary to restore the reduced-LE-size phenotype in Munc13-4–KO cells (Figure 4). Of importance, the Munc13-4-C2A*C2B* mutant, which lacks calcium-dependent binding to syntaxin 7, was unable to restore the wild-type phenotype, further supporting that the binding of Munc13-4 to this SNARE is important for calcium-dependent LE fusion.

Extensive studies using rat liver lysosomes and late endosomes elucidated the roles played by SNAREs in endosomal maturation (Mullock *et al.*, 1989; Pryor *et al.*, 2000). These studies showed that syntaxin 7 regulates both LE homotypic and LE–lysosome heterotypic fusion (Mullock *et al.*, 2000; Ward *et al.*, 2000). In addition, VAMP7 and VAMP8 were also shown to be essential for the membrane fusion events in the endocytic pathway (Pryor *et al.*, 2004). Roles in autophagosome–endolysosome fusion (Furuta *et al.*, 2010; Diao *et al.*, 2015) and exocytosis (Wang *et al.*, 2007) were also proposed for VAMP8. In neutrophils, using inhibitory antibodies, one study suggested that VAMP7 but not VAMP8 regulates exocytosis (Logan *et al.*, 2006). A possible role for VAMP8 in these cells has been elusive. Here we show for the first time that syntaxin 7, VAMP8, and Munc13-4 are able to form a complex that coimmunoprecipitates in a calcium-dependent manner and that Munc13-4 calcium-binding-deficient mutants that impair these interactions are unable to rescue the late endosomal enlarged phenotype observed in Munc13-4–KO neutrophils (Figure 4), supporting a role for syntaxin 7, VAMP8, and Munc13-4 in LE maturation in neutrophils.

Two independent observations presented in this study suggest that the fusion of degradative enzyme–containing compartments with late endosomes is defective in Munc13-4–KO neutrophils. First, using a self-quenched fluorogenic probe that is internalized through the endocytic pathway and becomes fluorescent upon digestion in degradative compartments, we showed that Munc13-4–KO neutrophils have impaired degradation of endocytic substrates (Figure 6D). Second, our results showing lower levels of colocalization of the LE signaling receptor TLR9 with cathepsin G in Munc13-4–KO cells and no significant increase in colocalization in CpG-treated Munc13-4–KO neutrophils compared with unstimulated cells (Figure 6) further support the idea that the fusion of late endosomes with degradative enzyme–containing lysosomes is impaired in the absence of Munc13-4. Late endosomal TLR9 activation and signaling are central mechanisms in innate immunity, inflammation, and autoimmunity. These are fundamental processes that not only help to shape appropriate cellular responses during infections but also modulate the cellular functions at the inflammatory site. Here we show that Munc13-4 directly regulates TLR9-initiated signaling and TLR9-dependent up-regulation of the neutrophil adhesion molecule and receptor CD11b at the plasma membrane, a process that is impaired in Munc13-4–deficient cells and inhibited by chloroquine treatment in wild-type cells. Thus our data highlight a novel mechanism of endosomal function mediated by Munc13-4, which appears to be an essential component of the machinery that regulates TLR9 activation. Based on these data, it is tempting to propose that putative interference with the role of Munc13-4 in LE maturation could potentially decrease inflammation by impairing TLR9-dependent signaling and TLR9-initiated proinflammatory functions.

Taking our results together, we showed a novel interaction of Munc13-4 with the late endosomal SNARE syntaxin 7, demonstrated that this is an important process for late endosomal maturation, and suggested that Munc13-4 is a good candidate to mediate calcium sensing in this process. Furthermore, we showed that late endosomal signaling and the control of important regulatory molecules for host–pathogen interaction are impaired in the absence of Munc13-4, further supporting the idea that Munc13-4 is a central regulator of the late endocytic machinery and associated innate immune cellular functions.

MATERIALS AND METHODS

Animals

C57BL/6 *Munc13-4*$^{jinx/jinx}$ mice (hereafter referred to as *Jinx*; Crozat *et al.*, 2007) and their parental strain, C57BL/6 (wild type), were used. Mice (6–12 wk old) were maintained in a pathogen-free environment and had access to food and water ad libitum. All animal studies were performed in compliance with the Department of Health and Human Services Guide for the Care and Use of Laboratory Animals. All studies were conducted according to National Institutes of Health and institutional guidelines and with approval of the animal review board at Scripps Research Institute.

Expression vectors and mutagenesis

GFP-Vamp8, syntaxin 7, syntaxin 17, syntaxin 18, and Vti1b were obtained from Addgene (Cambridge, MA). Histidine-tagged syntaxin 3 and syntaxin 4 were obtained from Addgene and then subcloned into the EGFP-C1 vector (Clontech Laboratories, Mountain View, CA). mCherry-Munc13-4 and flag-Munc13-4 were obtained from Genecopoeia (Rockville, MD). Munc13-4 mutagenesis was carried out using QuikChange Site-Directed Mutagenesis Kit (Agilent, Santa Clara, CA) following the manufacturer's instructions. The primers used for mutagenesis were 5′-attctgggcaaaAatgtcagtgggttcagcAacccctactgcc-3′ and 5′-ggcagtaggggtTgctgaacccactgacatTtttgcccagaat-3′ for the C2A domain and 5′-ctgctgcccctgAactccaatggctccagcAacccctttgtcc-3′ and 5′-ggacaaaggggtTgctggagccattggagtTcaggggcagcag-3′ for the C2B domain.

Binding assay

For TR-FRET binding assays, 293T cell lysates expressing Flag-tagged Munc13-4 and GFP-tagged SNAREs were used to evaluate protein–protein interactions. Where indicated, reactions were

carried out in relaxation buffer (100 mM KCl, 3 mM NaCl, 3.5 mM $MgCl_2$, 10 mM 4-(2-hydroxyethyl)-1-piperazineethanesulfonic acid) in the presence of 100 µM $CaCl_2$ or 200 µM ethylene glycol tetraacetic acid (EGTA). The reactions were started by addition of the terbium cryptate–conjugated anti-Flag antibody (Cisbio, Bedford, MA) at 15 pg/µl in a final volume of 10 µl following the manufacturer's instructions. The reactions were carried out at 21°C, and the emission ratio of the acceptor (GFP, 520 nm) to the donor (Tb, 490 nm) was read using an Envision plate reader.

Antibodies

Primary antibodies used for Western blotting and immunofluorescent staining were as follows: anti–syntaxin 7 (AF5478; R&D Systems), VAMP8 (104302; Synaptic Systems, Goettingen, Germany), MPO (HM1051; Hycult Biotech, Uden, Netherlands), TLR9 (PA5-20203; Thermo Fisher Scientific, Asheville, NC), phosphorylated Erk and total Erk (9101, 9202; Cell Signaling Technology, Danvers, MA), phosphorylated P38 and total P38 (9211, 9212; Cell Signaling Technology), Flag (CGAB-DDK; Genecopoeia), GFP (A6455; Life Technologies, Carlsbad, CA), LAMP1 (sc-19992; Santa Cruz Biotechnology, Santa Cruz, CA), Myc (sc-40; Santa Cruz Biotechnology), Munc13-4 (described previously; Brzezinska *et al.*, 2008), and anti-Rab7 (D95F2; Cell Signaling Technology).

SDS–PAGE, Western blotting, and immunoprecipitation

Proteins were separated by gel electrophoresis using NuPAGE gels and 3-(*N*-morpholino)propanesulfonic acid buffer (Life Technologies). Proteins were transferred onto nitrocellulose membranes for 120 min at 100 V at 4°C. The membranes were blocked with phosphate-buffered saline (PBS) containing 5% (wt/vol) blotting-grade nonfat dry milk blocker (Rockland, Limerick, PA) and 0.05% (wt/vol) Tween 20. Proteins were detected by probing the membranes with the indicated primary antibodies at appropriate dilutions and using a detection system consisting of horseradish peroxidase–conjugated secondary antibodies (Bio-Rad Laboratories, Hercules, CA) and the chemiluminescence substrates SuperSignal, WestPico, and WestFemto (Thermo Scientific) and then visualized using Hyperfilm (Denville Scientific, Holliston, MA). For immunoprecipitation assay, cells were lysed either by nitrogen cavitation in relaxation buffer supplemented with 1% NP-40 or directly using RIPA buffer (50 mM Tris/HCl, 150 mM NaCl, 0.1% SDS, 0.5% sodium deoxycholate, 1% NP-40), the samples were cleared by centrifugation, and the supernatants were then incubated with anti–M2 agarose beads (Sigma-Aldrich, St. Louis, MO) at 4°C with rotation overnight. After three washes with lysis buffer, the immunoprecipitates were subjected to Western blotting.

Mouse neutrophil isolation

Bone marrow–derived neutrophils were isolated using a Percoll gradient fractionation system as described (Johnson *et al.*, 2012). A three-layer Percoll gradient was used (52, 64, and 72%), and neutrophils were isolated from the 64/72% interface, washed in PBS, and used in all the assays.

Immunofluorescence, confocal microscopy, and colocalization analysis

Neutrophils were seeded on untreated coverglasses (Cole-Parmer, Vernon Hills, IL) and incubated at 37°C for 1 h, then fixed with 1.5% paraformaldehyde for 15 min or with 4% PAF for 10 min, permeabilized with 0.02% saponin, and blocked with 1% BSA in PBS. Samples were labeled with the indicated primary antibodies overnight at 4°C in the presence of 0.02% saponin and 1% BSA. Samples were washed and subsequently incubated with the appropriate combinations of Alexa Fluor (488, 594, or 633)–conjugated donkey anti-rabbit, anti-rat, anti-sheep, or anti-mouse secondary antibodies (Life Technologies). Samples were analyzed with a Zeiss LSM 710 laser scanning confocal microscope attached to a Zeiss Observer Z1 microscope at 21°C, using a 63× oil Plan Apo, 1.4 numerical aperture (NA) objective. Images were collected using ZEN-LSM software and processed using ImageJ (National Institutes of Health, Bethesda, MD) and Photoshop CS4 (Adobe). Analysis of colocalization was performed using ZEN software.

Nucleofection

Mouse neutrophil nucleofection was carried out using the 4D-Nucleofector X Unit system (Lonza) following the manufacturer's instructions. In brief, mouse neutrophils were counted, and 1×10^6 cells were resuspended in 20 µl of Lonza P3 solution with 0.1–1 µg of DNA and the solutions were transferred into the X Unit and then subjected to nucleofection in the 4D-Nucleofector using program EA-100. The cells were then resuspended in phenol red–free RPMI (Life Technologies) and seeded into four-chamber 35-mm glass-bottom dishes (No. 1.5 borosilicate coverglass; In Vitro Scientific). Cells were incubated at 37°C for at least 4 h before microscopy analysis. For the CQ treatment experiments, the transfected cells were left to recover for 1 h after transfections and then incubated in the presence of 50 µM CQ for 4 h before TIRFM analysis.

TIRFM

TIRFM experiments were performed using a 100×/1.45 NA TIRF objective (Nikon Instruments, Melville, NY) on a Nikon TE2000U microscope custom modified with a TIRF illumination module as described (Johnson *et al.*, 2012). Images were acquired on a 14-bit, cooled charge-coupled device (CCD) camera (Hamamatsu) controlled through NIS-Elements software. The images were recorded using 300- to 500-ms exposures, depending on the fluorescence intensity of the sample. Images were analyzed using ImageJ software to measure late endosome diameter. Specifically, the longest diameter of the LAMP1-positive large vesicles was drawn manually using the Straight Line tool, and the length was measured using the Measure tool. The 10 biggest LAMP1-positive late endosomes (if applicable) were measured in each cell.

Immuno–electron microscopy

Cells were fixed using 4% paraformaldehyde (Electron Microscopy Sciences, Hatfield, PA) in 0.1 M phosphate buffer, pH 7.4, overnight at 4°C. Fixed cells were washed with 0.15 M glycine/phosphate buffer, embedded in 10% gelatin/phosphate buffer, and infused with 2.3 M sucrose/phosphate buffer overnight at 4°C. Frozen sections of 80–90 nm were placed onto Formvar- and carbon-coated copper grids. Grids were placed on 2% gelatin at 37°C for 20 min and rinsed with 0.15 M glycine/PBS, and the sections were blocked using 1% cold-water fish-skin gelatin. Samples were incubated with rat anti-LAMP1 antibody (1:50 dilution) at room temperature for 1 h, followed by incubation with gold-conjugated goat anti-rat immunoglobulin G (IgG) and IgM (1:25 dilution; Jackson ImmunoResearch) at room temperature for 45 min. Grids were viewed using a JEOL 1200EX II transmission electron microscope and photographed using a Gatan digital camera.

Superresolution microscopy

STORM was performed as described previously (Napolitano *et al.*, 2015). Briefly, cells were labeled with anti-LAMP1, anti–Munc13-4,

and anti–syntaxin 7 primary antibodies and Alexa 647– and Alexa 488–conjugated secondary antibodies. Samples were suspended in freshly prepared STORM buffer (50 mM Tris, pH 8.0, 10 mM NaCl, 10% glucose, 0.1 M mercaptoethanolamine [cysteamine; Sigma-Aldrich], 56 U/ml glucose oxidase [from *Aspergillus niger*; Sigma-Aldrich], and 340 U/ml catalase [from bovine liver; Sigma-Aldrich]) and imaged on a Nikon Ti superresolution microscope. Samples were imaged using a 100×/1.49 NA Apo TIRF objective either with or without TIRF illumination. Images were collected on an Andor IXON3 Ultra DU897 electron-multiplying CCD camera using the multicolor continuous mode setting in the Nikon Elements software. Power on the 488- and 647-nm lasers was adjusted to enable collection of 50–300 molecules per 256 × 256 camera pixel frame at appropriate threshold settings for each channel. Collection was stopped after a sufficient number of frames were collected (usually yielding (1–2) × 10^6 molecules), and the superresolution images were reconstructed with the Nikon STORM software.

Neutrophil stimulation and flow cytometry analysis

For flow cytometry studies, 1 × 10^6 mouse neutrophils were resuspended in phenol red–free RPMI and treated with 50 μM CQ (Sigma-Aldrich) or vehicle before stimulation with 10 μM fMLP (Calbiotech, Spring Valley, CA) for 10 min or with 10 ng/ml granulocyte macrophage colony stimulating factor (GM-CSF; Shenandoah Biotechnology) for 30 min and 5 μM CpG (ODN 1826; InvivoGen) for 1 h at 37°C. To evaluate the plasma membrane expression of CD11b in mouse neutrophils, the live cells were blocked in PBS with 1% BSA and stained with anti–mouse-CD11b-Alexa 647 (clone M1/70; BD Biosciences, San Jose, CA). Ly-6G was also stained to gate the neutrophil population using anti–mouse-Ly-6G-fluorescein isothiocyanate (clone 1A8; BD Biosciences). The cells were then washed and fixed in 1% paraformaldehyde in PBS. The samples were analyzed using a BD LSR II flow cytometer (BD Biosciences), and the data were processed using FlowJo (Ashland, OR) software. To evaluate LE-degradative capacity, neutrophils were transfected for the expression of EGFP-LAMP1 and incubated in the presence of 40 μg/ml DQ-BSA (Life Technologies) for 4 h. Live neutrophils were imaged by pTIRFM. Next the cells were fixed, imaged by confocal microscopy, and quantified using ImageJ. In some experiments, the fluorescence intensity from digested DQ-BSA was quantified by flow cytometry.

Mitogen-activated protein kinase phosphorylation

Mouse neutrophils were treated with 10 ng/ml GM-CSF for 30 min before stimulation with 5 μM CpG for the indicated times. The cells were lysed with RIPA buffer supplemented with protease inhibitor cocktail (Roche) and subjected to Western blotting using the indicated antibodies. Where indicated, the cells were treated with the mitogen-activated protein kinase inhibitor PD98059 (50 μM; Calbiotech) or dimethyl sulfoxide for 30 min in the presence or absence of 10 ng/ml GM-CSF and subsequently stimulated with 5 μM CpG before analysis. Erk phosphorylation was quantified using ImageJ. The phosphorylated Erk intensity values were first normalized to total Erk and then normalized to the value of the sample labeled "wild type, CpG 10 min."

Statistical analysis

Data are presented as means, and error bars correspond to SEMs, unless otherwise indicated. Statistical significance was determined using the unpaired Student's *t* test or the analysis of variance test using GraphPad InStat (version 3) or Excel software, and graphs were made using GraphPad Prism (version 4) software. Peirce's criterion and Grubbs' test were used to determine statistical outliers.

ACKNOWLEDGMENTS

We thank Beverley Ellis for editing, corrections, and comments and Timo Meerloo (University of California, San Diego) for help with immuno–electron microscopy. This work was supported by U.S. Public Health Service Grants HL088256 and GM105894 to S.D.C. and American Heart Association fellowships to M.R. and J.M. J.Z. is a Fellow of the Cystinosis Research Foundation.

REFERENCES

Antonin W, Holroyd C, Fasshauer D, Pabst S, Von Mollard GF, Jahn R (2000). A SNARE complex mediating fusion of late endosomes defines conserved properties of SNARE structure and function. EMBO J 19, 6453–6464.

Berger M, Wetzler E, August JT, Tartakoff AM (1994). Internalization of type 1 complement receptors and de novo multivesicular body formation during chemoattractant-induced endocytosis in human neutrophils. J Clin Invest 94, 1113–1125.

Borregaard N, Lollike K, Kjeldsen L, Sengelov H, Bastholm L, Nielsen MH, Bainton DF (1993). Human neutrophil granules and secretory vesicles. Eur J Haematol 51, 187–198.

Boswell KL, James DJ, Esquibel JM, Bruinsma S, Shirakawa R, Horiuchi H, Martin TF (2012). Munc13-4 reconstitutes calcium-dependent SNARE-mediated membrane fusion. J Cell Biol 197, 301–312.

Brumell JH, Volchuk A, Sengelov H, Borregaard N, Cieutat AM, Bainton DF, Grinstein S, Klip A (1995). Subcellular distribution of docking/fusion proteins in neutrophils, secretory cells with multiple exocytic compartments. J Immunol 155, 5750–5759.

Brzezinska AA, Johnson JL, Munafo DB, Crozat K, Beutler B, Kiosses WB, Ellis BA, Catz SD (2008). The Rab27a effectors JFC1/Slp1 and Munc13–4 regulate exocytosis of neutrophil granules. Traffic 9, 2151–2164.

Bucci C, Thomsen P, Nicoziani P, McCarthy J, van Deurs B (2000). Rab7: a key to lysosome biogenesis. Mol Biol Cell 11, 467–480.

Caplan S, Hartnell LM, Aguilar RC, Naslavsky N, Bonifacino JS (2001). Human Vam6p promotes lysosome clustering and fusion in vivo. J Cell Biol 154, 109–122.

Catz SD (2013). Regulation of vesicular trafficking and leukocyte function by Rab27 GTPases and their effectors. J Leukoc Biol 94, 613–622.

Chapman RE, Munro S (1994). Retrieval of TGN proteins from the cell surface requires endosomal acidification. EMBO J 13, 2305–2312.

Cieutat AM, Lobel P, August JT, Kjeldsen L, Sengelov H, Borregaard N, Bainton DF (1998). Azurophilic granules of human neutrophilic leukocytes are deficient in lysosome-associated membrane proteins but retain the mannose 6-phosphate recognition marker. Blood 91, 1044–1058.

Clague MJ, Urbe S, Aniento F, Gruenberg J (1994). Vacuolar ATPase activity is required for endosomal carrier vesicle formation. J Biol Chem 269, 21–24.

Crozat K, Hoebe K, Ugolini S, Hong NA, Janssen E, Rutschmann S, Mudd S, Sovath S, Vivier E, Beutler B (2007). Jinx, an MCMV susceptibility phenotype caused by disruption of Unc13d: a mouse model of type 3 familial hemophagocytic lymphohistiocytosis. J Exp Med 204, 853–863.

Dell'Angelica EC, Mullins C, Caplan S, Bonifacino JS (2000). Lysosome-related organelles. FASEB J 14, 1265–1278.

Diao J, Liu R, Rong Y, Zhao M, Zhang J, Lai Y, Zhou Q, Wilz LM, Li J, Vivona S, *et al.* (2015). ATG14 promotes membrane tethering and fusion of autophagosomes to endolysosomes. Nature 520, 563–566.

Egesten A, Breton-Gorius J, Guichard J, Gullberg U, Olsson I (1994). The heterogeneity of azurophil granules in neutrophil promyelocytes: immunogold localization of myeloperoxidase, cathepsin G, elastase, proteinase 3, and bactericidal/permeability increasing protein. Blood 83, 2985–2994.

Elstak ED, Neeft M, Nehme NT, Voortman J, Cheung M, Goodarzifard M, Gerritsen HC, vBEH PM, Callebaut I, de Saint BG, van der SP (2011). The munc13–4-rab27 complex is specifically required for tethering secretory lysosomes at the plasma membrane. Blood 118, 1570–1578.

Feldmann J, Callebaut I, Raposo G, Certain S, Bacq D, Dumont C, Lambert N, Ouachee-Chardin M, Chedeville G, Tamary H, *et al.* (2003). Munc13-4 is essential for cytolytic granules fusion and is mutated in a form of familial hemophagocytic lymphohistiocytosis (FHL3). Cell 115, 461–473.

Forsyth CB, Plow EF, Zhang L (1998). Interaction of the fungal pathogen Candida albicans with integrin CD11b/CD18: recognition by the I domain is modulated by the lectin-like domain and the CD18 subunit. J Immunol 161, 6198–6205.

Furuta N, Fujita N, Noda T, Yoshimori T, Amano A (2010). Combinational soluble N-ethylmaleimide-sensitive factor attachment protein receptor proteins VAMP8 and Vti1b mediate fusion of antimicrobial and canonical autophagosomes with lysosomes. Mol Biol Cell 21, 1001–1010.
Goishi K, Mizuno K, Nakanishi H, Sasaki T (2004). Involvement of Rab27 in antigen-induced histamine release from rat basophilic leukemia 2H3 cells. Biochem Biophys Res Commun 324, 294–301.
Gruenberg J, Stenmark H (2004). The biogenesis of multivesicular endosomes. Nat Rev Mol Cell Biol 5, 317–323.
Gruenberg J, van der Goot FG (2006). Mechanisms of pathogen entry through the endosomal compartments. Nat Rev Mol Cell Biol 7, 495–504.
Gutierrez MG, Munafo DB, Beron W, Colombo MI (2004). Rab7 is required for the normal progression of the autophagic pathway in mammalian cells. J Cell Sci 117, 2687–2697.
Hacker H, Mischak H, Miethke T, Liptay S, Schmid R, Sparwasser T, Heeg K, Lipford GB, Wagner H (1998). CpG-DNA-specific activation of antigen-presenting cells requires stress kinase activity and is preceded by non-specific endocytosis and endosomal maturation. EMBO J 17, 6230–6240.
Huotari J, Helenius A (2011). Endosome maturation. EMBO J 30, 3481–3500.
Johnson JL, Hong H, Monfregola J, Catz SD (2011). Increased survival and reduced neutrophil infiltration of the liver in Rab27a- but not Munc13-4-deficient mice in lipopolysaccharide-induced systemic inflammation. Infect Immun 79, 3607–3618.
Johnson JL, Hong H, Monfregola J, Kiosses WB, Catz SD (2010). MUNC13-4 restricts motility of RAB27A-expressing vesicles to facilitate lipopolysaccharide-induced priming of exocytosis in neutrophils. J Biol Chem 286, 5647–5656.
Johnson JL, Monfregola J, Napolitano G, Kiosses WB, Catz SD (2012). Vesicular trafficking through cortical actin during exocytosis is regulated by the Rab27a effector JFC1/Slp1 and the RhoA-GTPase-activating protein Gem-interacting protein. Mol Biol Cell 23, 1902–1916.
Kim BY, Kramer H, Yamamoto A, Kominami E, Kohsaka S, Akazawa C (2001). Molecular characterization of mammalian homologues of class C Vps proteins that interact with syntaxin-7. J Biol Chem 276, 29393–29402.
Klebanoff SJ (2005). Myeloperoxidase: friend and foe. J Leukoc Biol 77, 598–625.
Klionsky DJ, Abeliovich H, Agostinis P, Agrawal DK, Aliev G, Askew DS, Baba M, Baehrecke EH, Bahr BA, Ballabio A, *et al.* (2008). Guidelines for the use and interpretation of assays for monitoring autophagy in higher eukaryotes. Autophagy 4, 151–175.
Koch H, Hofmann K, Brose N (2000). Definition of Munc13-homology-domains and characterization of a novel ubiquitously expressed Munc13 isoform. Biochem J 349, 247–253.
Kuijpers TW, Tool AT, van der Schoot CE, Ginsel LA, Onderwater JJ, Roos D, Verhoeven AJ (1991). Membrane surface antigen expression on neutrophils: a reappraisal of the use of surface markers for neutrophil activation. Blood 78, 1105–1111.
Lee WL, Harrison RE, Grinstein S (2003). Phagocytosis by neutrophils. Microbes Infect 5, 1299–1306.
Logan MR, Lacy P, Odemuyiwa SO, Steward M, Davoine F, Kita H, Moqbel R (2006). A critical role for vesicle-associated membrane protein-7 in exocytosis from human eosinophils and neutrophils. Allergy 61, 777–784.
Luzio JP, Gray SR, Bright NA (2010). Endosome-lysosome fusion. Biochem Soc Trans 38, 1413–1416.
Luzio JP, Pryor PR, Bright NA (2007). Lysosomes: fusion and function. Nat Rev Mol Cell Biol 8, 622–632.
Matsuo H, Chevallier J, Mayran N, Le Blanc I, Ferguson C, Faure J, Blanc NS, Matile S, Dubochet J, Sadoul R, *et al.* (2004). Role of LBPA and Alix in multivesicular liposome formation and endosome organization. Science 303, 531–534.
Menager MM, Menasche G, Romao M, Knapnougel P, Ho CH, Garfa M, Raposo G, Feldmann J, Fischer A, de Saint BG (2007). Secretory cytotoxic granule maturation and exocytosis require the effector protein hMunc13-4. Nat Immunol 8, 257–267.
Monfregola J, Johnson JL, Meijler MM, Napolitano G, Catz SD (2012). MUNC13-4 protein regulates the oxidative response and is essential for phagosomal maturation and bacterial killing in neutrophils. J Biol Chem 287, 44603–44618.
Moreland JG, Fuhrman RM, Pruessner JA, Schwartz DA (2002). CD11b and intercellular adhesion molecule-1 are involved in pulmonary neutrophil recruitment in lipopolysaccharide-induced airway disease. Am J Respir Cell Mol Biol 27, 474–480.
Mudrakola HV, Zhang K, Cui B (2009). Optically resolving individual microtubules in live axons. Structure 17, 1433–1441.
Mullock BM, Branch WJ, van Schaik M, Gilbert LK, Luzio JP (1989). Reconstitution of an endosome-lysosome interaction in a cell-free system. J Cell Biol 108, 2093–2099.
Mullock BM, Smith CW, Ihrke G, Bright NA, Lindsay M, Parkinson EJ, Brooks DA, Parton RG, James DE, Luzio JP, Piper RC (2000). Syntaxin 7 is localized to late endosome compartments, associates with Vamp 8, and Is required for late endosome-lysosome fusion. Mol Biol Cell 11, 3137–3153.
Murk JL, Posthuma G, Koster AJ, Geuze HJ, Verkleij AJ, Kleijmeer MJ, Humbel BM (2003). Influence of aldehyde fixation on the morphology of endosomes and lysosomes: quantitative analysis and electron tomography. J Microsc 212, 81–90.
Napolitano G, Johnson JL, He J, Rocca CJ, Monfregola J, Pestonjamasp K, Cherqui S, Catz SD (2015). Impairment of chaperone-mediated autophagy leads to selective lysosomal degradation defects in the lysosomal storage disease cystinosis. EMBO Mol Med 7, 158–174.
Neeft M, Wieffer M, de Jong AS, Negroiu G, Metz CH, van LA, Griffith J, Krijgsveld J, Wulffraat N, Koch H, *et al.* (2005). Munc13-4 is an effector of rab27a and controls secretion of lysosomes in hematopoietic cells. Mol Biol Cell 16, 731–741.
Peters C, Mayer A (1998). Ca2+/calmodulin signals the completion of docking and triggers a late step of vacuole fusion. Nature 396, 575–580.
Pivot-Pajot C, Varoqueaux F, de Saint BG, Bourgoin SG (2008). Munc13-4 regulates granule secretion in human neutrophils. J Immunol 180, 6786–6797.
Poole B, Ohkuma S (1981). Effect of weak bases on the intralysosomal pH in mouse peritoneal macrophages. J Cell Biol 90, 665–669.
Pryor PR, Mullock BM, Bright NA, Gray SR, Luzio JP (2000). The role of intraorganellar Ca(2+) in late endosome-lysosome heterotypic fusion and in the reformation of lysosomes from hybrid organelles. J Cell Biol 149, 1053–1062.
Pryor PR, Mullock BM, Bright NA, Lindsay MR, Gray SR, Richardson SC, Stewart A, James DE, Piper RC, Luzio JP (2004). Combinatorial SNARE complexes with VAMP7 or VAMP8 define different late endocytic fusion events. EMBO Rep 5, 590–595.
Riddle SM, Vedvik KL, Hanson GT, Vogel KW (2006). Time-resolved fluorescence resonance energy transfer kinase assays using physiological protein substrates: applications of terbium-fluorescein and terbium-green fluorescent protein fluorescence resonance energy transfer pairs. Anal Biochem 356, 108–116.
Rink J, Ghigo E, Kalaidzidis Y, Zerial M (2005). Rab conversion as a mechanism of progression from early to late endosomes. Cell 122, 735–749.
Rizo J, Sudhof TC (1998). C2-domains, structure and function of a universal Ca2+-binding domain. J Biol Chem 273, 15879–15882.
Savina A, Fader CM, Damiani MT, Colombo MI (2005). Rab11 promotes docking and fusion of multivesicular bodies in a calcium-dependent manner. Traffic 6, 131–143.
Segal AW (2005). How neutrophils kill microbes. Annu Rev Immunol 23, 197–223.
Shirakawa R, Higashi T, Tabuchi A, Yoshioka A, Nishioka H, Fukuda M, Kita T, Horiuchi H (2004). Munc13-4 is a GTP-Rab27-binding protein regulating dense core granule secretion in platelets. J Biol Chem 279, 10730–10737.
Solinger JA, Spang A (2013). Tethering complexes in the endocytic pathway: CORVET and HOPS. FEBS J 280, 2743–2757.
Teng FY, Wang Y, Tang BL (2001). The syntaxins. Genome Biol 2, REVIEWS3012.
Tietz PS, Yamazaki K, LaRusso NF (1990). Time-dependent effects of chloroquine on pH of hepatocyte lysosomes. Biochem Pharmacol 40, 1419–1421.
Wang CC, Shi H, Guo K, Ng CP, Li J, Gan BQ, Chien Liew H, Leinonen J, Rajaniemi H, Zhou ZH, *et al.* (2007). VAMP8/endobrevin as a general vesicular SNARE for regulated exocytosis of the exocrine system. Mol Biol Cell 18, 1056–1063.
Wang H, Frelin L, Pevsner J (1997). Human syntaxin 7: a Pep12p/Vps6p homologue implicated in vesicle trafficking to lysosomes. Gene 199, 39–48.
Ward DM, Pevsner J, Scullion MA, Vaughn M, Kaplan J (2000). Syntaxin 7 and VAMP-7 are soluble N-ethylmaleimide-sensitive factor attachment protein receptors required for late endosome-lysosome and homotypic lysosome fusion in alveolar macrophages. Mol Biol Cell 11, 2327–2333.